

Integrate-and-Fire Neurons Driven by Correlated Stochastic Input

Emilio Salinas

esalinas@wfubmc.edu

Department of Neurobiology and Anatomy, Wake Forest University School of Medicine, Winston-Salem, NC 27157-1010, U.S.A.

Terrence J. Sejnowski

terry@salk.edu

Computational Neurobiology Laboratory, Howard Hughes Medical Institute, Salk Institute for Biological Studies, La Jolla, CA 92037, U.S.A., and Department of Biology, University of California at San Diego, La Jolla, CA 92093, U.S.A.

Neurons are sensitive to correlations among synaptic inputs. However, analytical models that explicitly include correlations are hard to solve analytically, so their influence on a neuron's response has been difficult to ascertain. To gain some intuition on this problem, we studied the firing times of two simple integrate-and-fire model neurons driven by a correlated binary variable that represents the total input current. Analytic expressions were obtained for the average firing rate and coefficient of variation (a measure of spike-train variability) as functions of the mean, variance, and correlation time of the stochastic input. The results of computer simulations were in excellent agreement with these expressions. In these models, an increase in correlation time in general produces an increase in both the average firing rate and the variability of the output spike trains. However, the magnitude of the changes depends differentially on the relative values of the input mean and variance: the increase in firing rate is higher when the variance is large relative to the mean, whereas the increase in variability is higher when the variance is relatively small. In addition, the firing rate always tends to a finite limit value as the correlation time increases toward infinity, whereas the coefficient of variation typically diverges. These results suggest that temporal correlations may play a major role in determining the variability as well as the intensity of neuronal spike trains.

1 Introduction ---

Cortical neurons are driven by thousands of synaptic inputs (Braitenberg & Schüz, 1997). Therefore, one way to understand the integration properties of a typical cortical neuron is to consider its total input as a stochastic

variable with given statistical properties and calculate the statistics of the response (Gerstein & Mandelbrot, 1964; Ricciardi, 1977, 1995; Tuckwell, 1988, 1989; Smith, 1992; Shinomoto, Sakai, & Funahashi, 1999; Tiesinga, José, & Sejnowski, 2000). A common practice is to assume that the total input has a gaussian distribution with given mean and variance and that samples taken at different times are uncorrelated. Input correlations make the statistics of the output spike trains quite difficult to calculate, even for simple model neurons. Ignoring the correlations may actually be a reasonable approximation if their timescale is much smaller than the average time interval between output spikes. However, in cortical neurons, factors like synaptic and membrane time constants, as well as synchrony in the input spike trains (see, for example, Nelson, Salin, Munk, Arzi, & Bullier, 1992; Steinmetz et al., 2000), give rise to a certain input correlation time τ_{corr} (Svirskis & Rinzel, 2000), and this may be of the same order of magnitude as the mean interspike interval of the evoked response. Therefore, the impact of temporal correlations needs to be characterized, at least to a first-order approximation. Some advances in this direction have been made from somewhat different points of view (Feng & Brown, 2000; Salinas & Sejnowski, 2000; Svirskis & Rinzel, 2000).

Here we first consider a simple integrate-and-fire model without a leak current in which the voltage is driven by a stochastic input until a threshold is exceeded, triggering a spike. The origins of this model go back to the work of Gerstein and Mandelbrot (1964), who studied a similar problem—without input correlations—and solved it, in the sense that they determined the probability density function for the interspike intervals (the times between consecutive action potentials). Our approach is similar in spirit, but the models differ in two important aspects. First, in their theoretical model, Gerstein and Mandelbrot did not impose a lower bound on the model neuron's voltage, so in principle it could become infinitely negative (note, however, that they did use a lower bound in their simulations). Second, they used an uncorrelated gaussian input with a given mean and variance, where the mean had to be positive; otherwise, the expected time between spikes became infinite. In contrast, we use a correlated binary input and impose a hard lower bound on the voltage of the model neuron, which roughly corresponds to an inhibitory reversal potential; we call it the barrier. When the barrier is set at a finite distance from the threshold, solving for the full probability density distribution of the firing time becomes difficult, but such a barrier has two advantages: the moments of the firing time may be calculated explicitly with correlated input, and the mean of the input may be arbitrary.

We also investigate the responses of the more common integrate-and-fire model that includes a leak current (Tuckwell, 1988; Troyer & Miller, 1997; Salinas & Sejnowski, 2000; Dayan & Abbott, 2001), driven by the same correlated stochastic input. In this case, however, the solutions for the moments of the firing time are obtained in terms of series expansions.

We calculate the response of these model neurons to a stochastic input with certain correlation time τ_{corr} . The underlying problem that we seek to capture and understand is this. The many inputs that drive a neuron may be correlated with one another; for example, they may exhibit some synchrony. The synchrony patterns may change dynamically (Steinmetz et al., 2000; Fries, Reynolds, Rorie, & Desimone, 2001; Salinas & Sejnowski, 2001), so the question is how these changes affect the response of a postsynaptic neuron. This problem is of considerable interest in the field (Maršálek, Koch, & Maunsell, 1997; Burkitt & Clark, 1999; Diesmann, Gewaltig, & Aertsen, 1999; Kisley & Gerstein, 1999; Feng & Brown, 2000; Salinas & Sejnowski, 2000, 2001). We look at this problem by collapsing all separate input streams into a single stochastic input with a given correlation time, which depends on the synchrony or correlation structure among those streams. Thus, the stochastic input that we consider is meant to reflect, in a simplified way, the total summed effect of the original input streams, taking into account their correlation structure. The precise mapping between these streams and the parameters of the stochastic input (mean, variance, and correlation time) are difficult to calculate analytically but qualitatively, one may expect higher synchrony to produce higher input variance (Salinas & Sejnowski, 2000, 2001; Feng & Brown, 2000) and longer correlation times between streams to produce larger values of τ_{corr} .

The methods applied here are related to random walk and diffusion models in physics (Feynman, Leighton, & Sands, 1963; Van Kampen, 1981; Gardiner, 1985; Berg, 1993) and are similar to those used earlier (Gerstein & Mandelbrot, 1964; Ricciardi, 1977, 1995; Shinomoto et al., 1999) to study the firing statistics of simple neuronal models in response to a temporally uncorrelated stochastic input (see Tuckwell, 1988, 1989; Smith, 1992, for reviews). Similar approaches have also been used recently to study neural populations (Nykamp & Tranchina, 2000; Haskell, Nykamp, & Tranchina, 2001). Here we extend such methods to the case of a correlated binary input. What we find is that an increase in τ_{corr} typically increases both the mean firing rate and the variability of the output spike trains, but the strength of these effects depends differentially on the relative values of the input mean and variance. In addition, the behaviors obtained as τ_{corr} becomes large are also different: the rate saturates, whereas the variability may diverge. Thus, neural responses may be strongly modulated through changes in the temporal correlations of their driving input.

2 The Nonleaky Integrate-and-Fire Model

This model neuron has a voltage V that changes according to the input that impinges on it, such that

$$\tau \frac{dV}{dt} = \mu_0 + X(t), \quad (2.1)$$

where μ_0 and τ are constants. The first term on the right, μ_0 , corresponds to a mean or steady component of the input—the drift—whereas the second term corresponds to the variable or stochastic component, which has zero mean. We refer to X as the fluctuating current, or simply the current. In this model, an action potential, or spike, is produced when V exceeds a threshold V_θ . After this, V is reset to an initial value V_{reset} , and the integration process continues evolving according to equation 2.1. This model is related to the leaky integrate-and-fire model (Tuckwell, 1988; Troyer & Miller, 1997; Salinas & Sejnowski, 2000; Dayan & Abbott, 2001) and to the Ornstein-Uhlenbeck process (Uhlenbeck & Ornstein, 1930; Ricciardi, 1977, 1995; Shinomoto et al., 1999), but is different because it lacks a term proportional to $-V$ in the right-hand side of equation 2.1 (see below). An additional and crucial constraint is that V cannot fall below a preset value, which acts as a barrier. This barrier is set at $V = 0$. This is a matter of convenience; the actual value makes no difference in the results. Thus, only positive values of V are allowed. Except for the barrier, this model neuron acts as a perfect integrator: it accumulates input samples in a way that is mostly independent of the value of V itself, where τ is the time constant of integration.

We examine the time T that it takes for V to go from reset to threshold; T is known as the first passage time and is the quantity whose statistics we wish to determine.

3 Stochastic Input

To complete the description of the model, we need to specify the statistics of the input X . We will consider two cases: one in which X is uncorrelated gaussian noise, so $X(t)$ and $X(t + \Delta t)$ are independent, and another where X is correlated noise, so $X(t)$ and $X(t + \Delta t)$ tend to be similar. The former is the traditional approach; the latter is novel and is probably a more accurate model of real input currents.

In both cases, we will make use of a binary random variable $Z(t)$, such that

$$Z = \begin{cases} +1 & \text{with probability } 1/2 \\ -1 & \text{with probability } 1/2 \end{cases} \quad (3.1)$$

The relationship between Z and X depends on whether X represents uncorrelated or correlated noise; this will be specified below. At this point, however, it is useful to describe the properties of Z .

The overall probabilities of observing a positive or a negative Z are the same and equal to $1/2$, which means that the random variable has zero mean and unit variance:

$$\bar{Z} = 0 \quad (3.2)$$

$$\overline{Z^2} = 1. \quad (3.3)$$

Here, the bar indicates an average over samples, or expectation. This, together with the correlation function, defines the statistics of Z . When input current X is uncorrelated gaussian noise, the Z variable is also uncorrelated, so

$$\overline{Z(t_1)Z(t_1 + t)} = \delta(t), \quad (3.4)$$

where δ is the Dirac delta function. Expression 3.4 means that any two samples observed at different times are independent. When input current X represents correlated noise, the Z variable is temporally correlated, in which case

$$\overline{Z(t_1)Z(t_1 + t)} = \exp\left(-\frac{|t|}{\tau_{corr}}\right). \quad (3.5)$$

Equation 3.5 means that the correlation between subsequent Z samples falls off exponentially with a time constant τ_{corr} . In this case, although the probabilities for positive and negative Z are equal, the conditional probabilities given prior observations are not. That is exactly what the correlation function expresses: samples taken close together in time tend to be more similar to each other than expected by chance, so the probability that the sample $Z(t + \Delta t)$ is positive is greater if the sample $Z(t)$ was positive than if it was negative.

In equation 3.5, a single quantity parameterizes the degree of correlation, τ_{corr} . This correlation time can also be expressed as a function of a single probability P_c , which is the probability that the sign of the next sample, $Z(t + \Delta t)$, is different from the sign of the previous one, $Z(t)$. The probability that the next sample has the same sign as the previous one is termed P_s and is equal to $1 - P_c$. For small Δt , the relationship between τ_{corr} and P_c is

$$P_c = \frac{\Delta t}{2\tau_{corr}}. \quad (3.6)$$

This can be seen as follows. First, calculate the correlation between consecutive Z samples directly in terms of P_c :

$$\begin{aligned} \overline{Z(t_1)Z(t_1 + \Delta t)} &= \frac{1}{2} [(1)(-1)P_c + (1)(1)P_s + (-1)(1)P_c + (-1)(-1)P_s] \\ &= 1 - 2P_c. \end{aligned} \quad (3.7)$$

The first term in the sum, for instance, corresponds to $Z(t) = 1$ and $Z(t + \Delta t) = -1$; since the probability that $Z(t) = 1$ is $1/2$ and the probability that the next sample has a different sign is P_c , the product $(1)(-1)$ has a probability $(1/2)P_c$. Similar calculations apply to the other three terms. Now calculate the same average by expanding equation 3.5 in a Taylor

series, using $t = \Delta t$. The resulting expression must be analogous to the equation above, and this leads to equation 3.6.

Finally, notice that as the correlation time becomes shorter and approaches Δt , $P_s \rightarrow 1/2$ and Z values separated by a fixed time interval tend to become independent. On the other hand, $P_s \rightarrow 1$ corresponds to a long correlation time, in which case the sequence of binary input samples consists of long stretches in which all samples are equal to $+1$ or -1 . Using the binary variable Z makes it possible to include correlations in the integrator model, and these can be varied by adjusting the value of P_c or, equivalently, τ_{corr} .

3.1 Discretizing Noise. The noisy current $X(t)$ is a continuous variable, but in order to proceed, it needs to be discretized. This is a subtle technical point, because the discretization depends on whether the noise is correlated.

Gaussian white noise can be approximated by setting X at time step j equal to

$$X_j = Z_j \frac{\sigma_0}{\sqrt{\Delta t}} = \pm \frac{\sigma_0}{\sqrt{\Delta t}}, \quad (3.8)$$

with equal probabilities for positive and negative values and with consecutive Z samples being independent. Here, the constant σ_0 measures the strength of the fluctuating current. In contrast, correlated noise can be approximated by setting X at time step j equal to

$$X_j = Z_j \sigma_1 = \pm \sigma_1, \quad (3.9)$$

where, in this case, consecutive Z values are not independent: the probability of the next Z changing sign is equal to P_c . The latter expression is relatively straightforward, but the former includes a $\sqrt{\Delta t}$ factor that may seem odd. The rationale for this is as follows.

The variance of the integral of X from 0 to t should be proportional to t ; that is an essential property of noise. For gaussian white noise, when time is a continuous variable, this property follows immediately from the fact that the correlation between X samples is a delta function (as in equation 3.4). With discretized time, we should be able to approximate the integral with a sum over consecutive samples, $\sum_j^N X_j \Delta t$, where $t = N \Delta t$. For gaussian white noise, the variance of this sum is

$$\Delta t^2 \sum_{j,k}^N \overline{X_j X_k} = \Delta t^2 \sum_{j,k}^N \delta_{ij} c^2 = c^2 t \Delta t. \quad (3.10)$$

Here, c is a constant and δ_{ij} is equal to 1 whenever $i = j$ and to 0 otherwise. The δ_{ij} appears because X samples are independent. To make this variance proportional to t and independent of the time step, the proportionality constant c should be divided by $\sqrt{\Delta t}$, as in equation 3.8. Note also that as

$\Delta t \rightarrow 0$, the sum approaches a gaussian random variable even if individual terms are binary, as a result of the central limit theorem.

On the other hand, when the noise is correlated, the analogous calculation involves a correlation function with a finite amplitude. As a consequence, the variance of the sum of X samples ends up being independent of Δt without the need of an additional factor. With an exponential correlation function, the variance of $\sum_j^N X_j \Delta t$ is equal to

$$2\sigma_1^2 \tau_{corr} \left[t - \tau_{corr} \left(1 - \exp\left(-\frac{t}{\tau_{corr}}\right) \right) \right], \quad (3.11)$$

which is proportional to τ_{corr} . Details of the calculation are omitted. The key point is that it uses equation 3.9 with an exponential correlation function, equation 3.5, and does not require an extra $\sqrt{\Delta t}$.

Appendixes A and B describe how random numbers with these properties can be generated in practice.

4 The Moments of T of the Nonleaky Neuron Driven by Uncorrelated Noise

First, we briefly review the formalism used to characterize the statistics of the first passage time when the input current is described by uncorrelated gaussian noise. Then we generalize these derivations to the case of correlated input, which is presented further below.

The quantity of interest is the random variable T , the time that it takes for the voltage V to go from reset to threshold. Its characterization depends on the probability density function $f(T, V)$, where $\Delta t f(T, V)$, is the probability that, starting from a voltage V , threshold is reached between T and $T + \Delta t$ time units later. The fluctuating input current in this case is described by gaussian white noise. To compute the density function f , equation 2.1 needs to be discretized first, so that time runs in steps of size Δt .

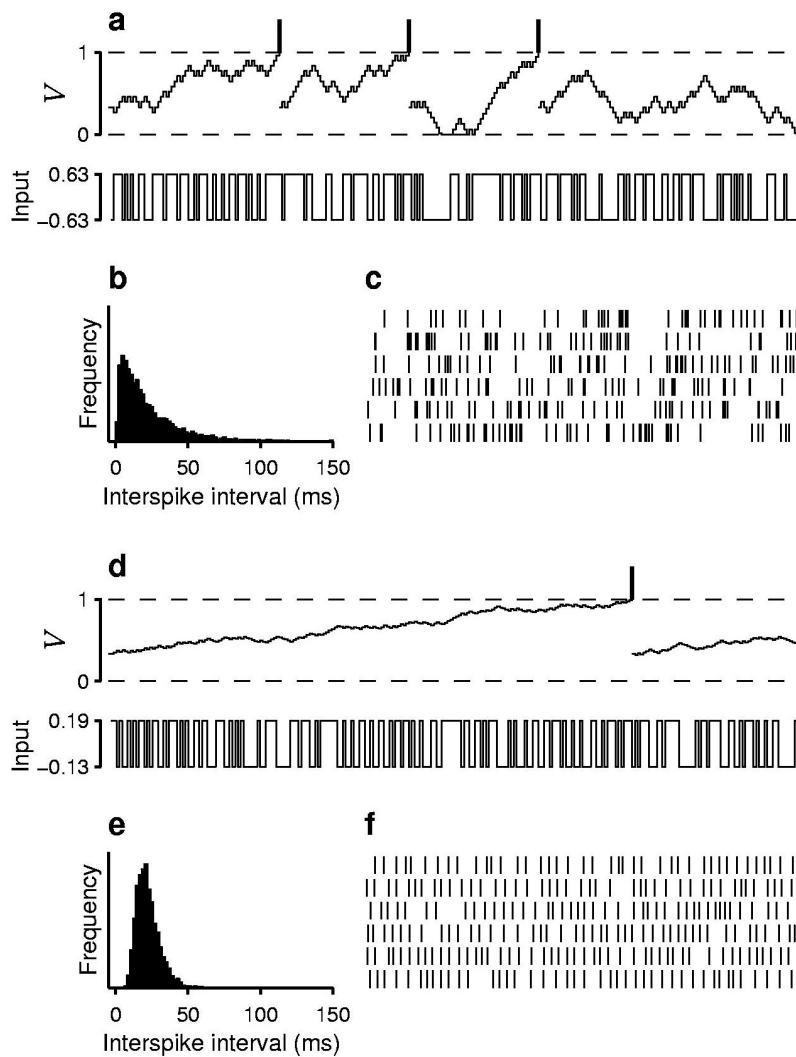
As shown above, when time is discretized, gaussian white noise can be approximated by setting X in each time step equal to $Z\sigma_0/\sqrt{\Delta t}$. Thus, for an uncorrelated gaussian current, the discretized version of equation 2.1 is

$$V(t + \Delta t) = V(t) + \left(\mu + \frac{\sigma}{\sqrt{\Delta t}} Z \right) \Delta t, \quad (4.1)$$

where $Z = \pm 1$ and consecutive samples are uncorrelated. Also, we have defined

$$\begin{aligned} \mu &\equiv \frac{\mu_0}{\tau} \\ \sigma &\equiv \frac{\sigma_0}{\tau}. \end{aligned} \quad (4.2)$$

Figure 1 shows examples of spike trains produced by the model when the input is binary and uncorrelated. When there is no drift ($\mu = 0$), as in Figures 1a through 1c, firing is irregular; the probability distribution of the times between spikes is close to an exponential (see Figure 1b), as for a Poisson process. Something different happens when there is a strong drift, as in Figures 1d through 1f: the evoked spike train is fairly regular, and the times between spikes cluster around a mean value (see Figure 1e). Thus, as observed before (Troyer & Miller, 1997; Salinas & Sejnowski, 2000), there



are two regimes: one in which the drift provides the main drive and firing is regular, and another in which the variance provides the main drive and firing is irregular. The quantitative dependence of the mean firing rate and variability on the input parameters μ , σ , and P_c is derived below.

4.1 Equations for the Moments of T . Now we proceed with the derivation of $f(T, V)$. The fundamental relationship that this function obeys is

$$f(T, V(t)) = \overline{f(T - \Delta t, V(t + \Delta t))}. \quad (4.3)$$

Here, as above, the bar indicates averaging over the input ensemble, or expectation. This equation describes how the probability of reaching threshold changes after a single time step: if at time t the voltage is V and T time units remain until threshold, then at time $t + \Delta t$, the voltage will have shifted to a new value $V(t + \Delta t)$ and, on average, threshold will be reached one Δt sooner. To proceed, substitute equation 4.1 into the above expression and average by including the probabilities for positive and negative input samples to obtain

$$f(T + \Delta t, V) = \frac{1}{2}f\left(T, V + \mu\Delta t + \sigma\sqrt{\Delta t}\right) + \frac{1}{2}f\left(T, V + \mu\Delta t - \sigma\sqrt{\Delta t}\right). \quad (4.4)$$

Here $V(t)$ is just V , and to simplify the next step we also made the shift $T \rightarrow T + \Delta t$. Next, expand each of the three f terms in Taylor series around $f(T, V)$. This gives rise to a partial derivative with respect to T on the left-hand side and to partial derivatives with respect to V on the right. In the

Figure 1: *Facing page.* Responses of the nonleaky integrate-and-fire model driven by stochastic, binary noise. Input samples are uncorrelated, so at each time step they are equally likely to be either positive or negative, regardless of previous values. (a) Sample voltage and input timecourses. Traces represent 25 ms of simulation time, with $\Delta t = 0.1$ ms. The top trace shows the model neuron's voltage V along with the spikes generated when V exceeds the threshold $V_\theta = 1$. After each spike, the voltage excursion restarts at $V_{reset} = 1/3$. The bottom traces show the total input $\mu + Z\sigma/\sqrt{\Delta t}$ at each time step, where Z may be either $+1$ or -1 . The input has zero mean, and firing is irregular. Parameters in equation 4.1 were $\mu = 0$, $\sigma = 0.2$. (b) Frequency histogram of interspike intervals from a sequence of approximately 4,000 spikes; bin size is 2 ms. Similar numbers were used in histograms of other figures. Here $\langle T \rangle = 22$ ms, $CV_{ISI} = 0.91$. (c) Spike raster showing 6 seconds of continuous simulation time; each line represents 1 second. The same parameters were used in *a* through *c*. Panels *d* through *f* have the same formats and scales as the respective panels above, except that $\mu = 0.03$ and $\sigma = 0.05$. The input has a strong positive drift, and firing is much more regular. In this case, $\langle T \rangle = 22$ ms, $CV_{ISI} = 0.35$.

latter case, second-order derivatives are needed to avoid cancelling of all the terms with σ . After simplifying the resulting expression, take the limit $\Delta t \rightarrow 0$ to obtain

$$\frac{\sigma^2}{2} \frac{\partial^2 f}{\partial V^2} + \mu \frac{\partial f}{\partial V} = \frac{\partial f}{\partial T}. \quad (4.5)$$

This has the general form of the Fokker-Planck equation that arises in the study of Brownian motion and diffusion processes (Van Kampen, 1981; Gardiner, 1985; Risken, 1996). In this case, it should satisfy the following boundary conditions. First,

$$\frac{\partial f(T, 0)}{\partial V} = 0, \quad (4.6)$$

which corresponds to the presence of the barrier at $V = 0$. Second,

$$f(T, V_\theta) = \delta(T), \quad (4.7)$$

which means that once threshold is reached, it is certain that a spike will occur with no further delay.

From equation 4.5 and these boundary conditions, expressions for the mean, variance, and higher moments of T may be obtained. To do this, multiply equation 4.5 by T^q and integrate each term over T . The result is an equation for the moment of T of order q :

$$\frac{\sigma^2}{2} \frac{d^2 \langle T^q \rangle}{dV^2} + \mu \frac{d \langle T^q \rangle}{dV} = -q \langle T^{q-1} \rangle, \quad (4.8)$$

where the angle brackets denote averaging over the probability distribution of T , that is,

$$\langle T^q \rangle = \langle T^q \rangle(V) = \int f(T, V) T^q dT. \quad (4.9)$$

The first equality above indicates that the moments of T are, in general, functions of V , although in some instances the explicit dependence will be omitted for brevity. The equation for the mean first passage time $\langle T \rangle$ is obtained when $q = 1$:

$$\frac{\sigma^2}{2} \frac{d^2 \langle T \rangle}{dV^2} + \mu \frac{d \langle T \rangle}{dV} = -1. \quad (4.10)$$

Similarly, the differential equation for the second moment follows by setting $q = 2$ in equation 4.8:

$$\frac{\sigma^2}{2} \frac{d^2 \langle T^2 \rangle}{dV^2} + \mu \frac{d \langle T^2 \rangle}{dV} = -2 \langle T \rangle. \quad (4.11)$$

Notice that to solve this equation, $\langle T \rangle$ needs to be computed first. Knowing the second moment of T is useful in quantifying the variability of the spike-train produced by the model neuron. One measure that is commonly used to evaluate spike-train variability is the coefficient of variation CV_{ISI} , which is equal to the standard deviation of the interspike intervals (the times between successive spikes) divided by their mean. Since the interspike interval is simply T ,

$$CV_{ISI} = \frac{\sqrt{\langle T^2 \rangle - \langle T \rangle^2}}{\langle T \rangle}. \quad (4.12)$$

For comparison, it is helpful to keep in mind that the CV_{ISI} of a Poisson process equals 1.

Boundary conditions for the moments of T are also necessary, but these can be obtained by the same procedure just described: multiply equations 4.6 and 4.7 by T^q and integrate over T . The result is

$$\begin{aligned} \frac{d\langle T^q \rangle}{dV}(V=0) &= 0 \\ \langle T^q \rangle(V=V_\theta) &= 0. \end{aligned} \quad (4.13)$$

4.2 General Solutions ($\mu \neq 0$). The solution to equation 4.10 may be found by standard methods. Taking into account the boundary conditions above with $q = 1$, we obtain

$$\begin{aligned} \langle T \rangle(V) &= \phi_1(V_\theta) - \phi_1(V) \\ \phi_1(x) &= \frac{x}{\mu} + \frac{\sigma^2}{2\mu^2} \exp\left(-\frac{2\mu x}{\sigma^2}\right). \end{aligned} \quad (4.14)$$

To obtain the mean time from reset to threshold, evaluate equations 4.14 at $V = V_{reset}$. After inserting these expressions into the right-hand side of equation 4.11 and imposing the corresponding boundary conditions, the solution for $\langle T^2 \rangle$ becomes

$$\begin{aligned} \langle T^2 \rangle(V) &= \phi_2(V_\theta) - \phi_2(V) \\ \phi_2(x) &= \left(\frac{2\phi_1(V_\theta)}{\mu} + \frac{\sigma^2}{\mu^3}\right)x - \frac{x^2}{\mu^2} + \\ &\quad + \left(\frac{\sigma^2\phi_1(V_\theta)}{\mu^2} + \frac{\sigma^4}{\mu^4} + \frac{\sigma^2 x}{\mu^3}\right) \exp\left(-\frac{2\mu x}{\sigma^2}\right), \end{aligned} \quad (4.15)$$

where ϕ_1 is the function defined in equations 4.14.

4.3 Solutions for Zero Drift ($\mu = 0$). The above expressions for $\langle T \rangle$ and $\langle T^2 \rangle$ are valid when μ is different from zero. When μ is exactly zero, the corresponding differential equations 4.10 and 4.11 become simpler, but the functional forms of the solutions change. In this case, the solution for $\langle T \rangle$ is

$$\begin{aligned} \langle T \rangle(V) &= \psi_1(V_\theta) - \psi_1(V) \\ \psi_1(x) &= \frac{x^2}{\sigma^2}. \end{aligned} \quad (4.16)$$

A very similar expression has been discussed before (Salinas & Sejnowski, 2000; see also Berg, 1993). In turn, the solution for $\langle T^2 \rangle$ becomes

$$\begin{aligned} \langle T^2 \rangle(V) &= \psi_2(V_\theta) - \psi_2(V) \\ \psi_2(x) &= \frac{2\psi_1(V_\theta)x^2}{\sigma^2} - \frac{x^4}{3\sigma^4}. \end{aligned} \quad (4.17)$$

These special solutions can also be obtained from the general expressions 4.14 and 4.15 by using a series representation for the exponentials and then taking the limit $\mu \rightarrow 0$.

Figures 2 and 3 compare these analytical solutions with computer simulations for a variety of values of σ and μ (see appendix C for details). The continuous lines in these figures correspond to analytic solutions. Equations 4.16 and 4.17 were used in Figure 2b, and equations 4.14 and 4.15 were used in the rest of the panels (as mentioned above, the expressions were evaluated at $V = V_{reset}$). The bottom rows in these figures plot the CV_{ISI} as defined in equation 4.12, and the top rows plot the mean firing rate r in spikes per second, where $r = 1/\langle T \rangle$. The dots in the graphs are the results of simulations. Each dot was obtained by first setting the values of μ and σ and then running the simulation until 1,000 spikes had been emitted; then $\langle T \rangle$ and $\langle T^2 \rangle$ were computed from the corresponding 1,000 values of T . The agreement between simulation and analytic results is very good for all combinations of μ and σ .

The results in Figures 2 and 3 confirm that firing in this model can be driven either by a continuous drift, in which case firing is regular, like a clock, or by the purely stochastic component of the input, in which case firing is irregular, like radioactive decay. For example, in Figure 3a, the mean rate rises steadily as a function of μ almost exactly along the line given by $r = \mu/(V_\theta - V_{reset})$, which is the solution for r when $\sigma = 0$ (see equation 4.14). The corresponding CV_{ISI} values stay very low, except when μ gets close to zero, in which case σ becomes relatively large. It is easy to see from equations 4.14 and 4.15 that when $\sigma = 0$, the CV_{ISI} becomes zero as well. In contrast, Figure 2b shows that when there is no drift and firing is driven by a purely stochastic input, the resulting spike train is much more irregular, with a CV_{ISI} slightly below one. Figure 2c shows an interesting

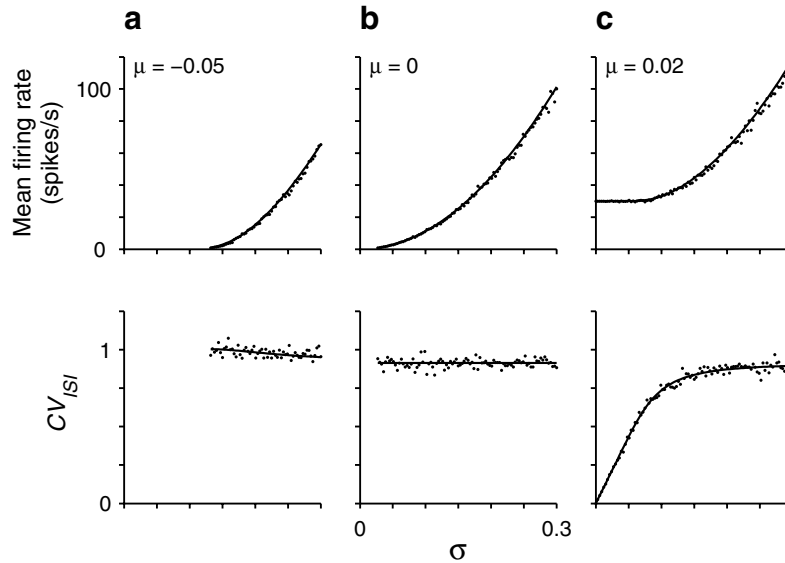


Figure 2: Mean firing rate and coefficient of variation for the nonleaky integrate-and-fire neuron driven by uncorrelated noise. Continuous lines are analytic expressions, and dots are results from computer simulations using gaussian white noise. Results are shown as functions of σ for the three values of μ indicated in the top-left corner of each panel. For each simulation data point, $\langle T \rangle$ and $\langle T^2 \rangle$ were calculated from spike trains containing 1,000 spikes (same in following figure). (a, c) The continuous lines were obtained from equations 4.14 and 4.15. (b) The continuous lines were obtained from equations 4.16 and 4.17.

intermediate case. As σ increases above zero, the firing rate changes little at first, but then, after a certain point around $\sigma = 0.1$, it increases steadily. In contrast, the CV_{ISI} increases most sharply precisely within the range of values at which the rate stays approximately constant, starting to saturate just as the firing rate starts to rise.

5 The Moments of T of the Nonleaky Neuron Driven by Correlated Noise

Correlated noise can also be approximated using a binary description. When there are correlations, changes in the sign of $X(t)$ occur randomly but with a characteristic timescale τ_{corr} (recall that X has zero mean). In this case, the key to approximate X with a binary variable is to capture the statistics of the transitions between positive and negative values. Intuitively, this may be thought as follows. A sample X is observed, and it is positive. On average, it will remain positive for another τ_{corr} time units approxi-

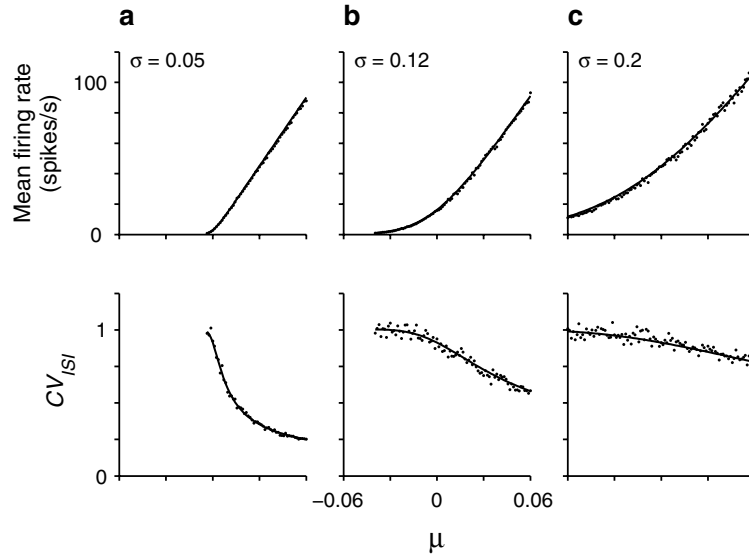


Figure 3: As in Figure 2, but the mean firing rate and coefficient of variation are plotted as functions of μ for the three values of σ indicated in the top-left corner of each panel. All continuous lines were obtained from equations 4.14 and 4.15.

mately. Therefore, in a time interval Δt longer than τ_{corr} , one would expect to see $\Delta t/(2\tau_{corr})$ sign changes; for instance, in a period of length $2\tau_{corr}$, one should see, on average, a single sign change. Thus, the probability that $X(t)$ and $X(t + \Delta t)$ have different signs, for small Δt , should be equal to $\Delta t/(2\tau_{corr})$. This is the quantity we called P_c above. A random process that changes states in this way gives rise to a correlation function described by an exponential, as in equation 3.5 (see appendix A), and has a finite variance.

For a correlated random current, the discretized version of equation 2.1 is

$$V(t + \Delta t) = V(t) + (\mu + \sigma Z) \Delta t, \quad (5.1)$$

where $Z = \pm 1$. Now, however, Z has an exponential correlation function, and although $+1$ and -1 are equally probable overall, the transitions between $+1$ and -1 do not have identical probabilities, as described earlier. As before, we have rescaled the mean and variance of the input:

$$\begin{aligned} \mu &\equiv \frac{\mu_0}{\tau} \\ \sigma &\equiv \frac{\sigma_1}{\tau}. \end{aligned} \quad (5.2)$$

However, we use σ_1 instead of σ_0 to note that the two quantities correspond to different noise models, correlated and uncorrelated, respectively. There is a subtle difference between them: the $\sqrt{\Delta t}$ factor is needed to discretize gaussian white noise but not correlated noise, so σ_1 and σ_0 end up having different units (see above).

Figures 4 and 5 show examples of spike trains produced by the model when the input is binary and temporally correlated. In Figure 4, the model has a negative drift, so firing is driven by the random fluctuations only. In Figures 4a and 4c, the correlation time is $\tau_{corr} = 1$ ms, and, as expected, on average the input changes sign every 2 ms (see Figure 4a, lower trace). When τ_{corr} is increased to 5 ms, the changes in sign occur approximately every 10 ms (see Figure 4d, lower trace). This gives rise to a large increase in mean firing rate and a smaller increase in CV_{ISI} , as can be seen by comparing the spike trains in Figures 4c and 4f. Note that μ and σ are the same for all panels. Figure 5 shows the effect of an identical change in correlation time on a model neuron that has a large positive drift. When $\tau_{corr} = 1$ ms, firing is regular (see Figure 5c). When τ_{corr} increases to 5 ms, there is no change in the mean firing rate, but the interspike intervals become much more variable (see Figure 5f). In both figures, long correlation times give rise to a sharp peak in the distribution of interspike intervals (see Figures 4e and 5e), which corresponds to a short interspike interval that appears very frequently. This short interval results when the input stays positive for a relatively long time, as illustrated by the two spikes in the voltage trace in Figure 4d. This interval is equal to $(V_\theta - V_{reset})/(\mu + \sigma)$, which is the minimum separation between spikes in the model given μ and σ . As the correlation time increases, a larger proportion of spikes separated by this interval is observed. For instance, for the parameters in Figures 4f and 5f, the minimum interval accounts approximately for 48% and 28%, respectively, of all interspike intervals.

Analytic solutions for the mean firing rate and the CV_{ISI} of the nonleaky model driven by correlated noise are derived in the following sections.

5.1 Equations for the Moments of T . In the case of correlated input, the probability that threshold is reached in T time units depends not only on the value of $V(t)$ but also on the value of $Z(t)$. If $Z(t)$ is, say, positive, then it is more likely that $Z(t + \Delta t)$ will also be positive, so we should expect threshold to be reached sooner when $Z(t)$ is positive than when it is negative. This means that now, instead of the single probability distribution f used before, two functions should be considered: $f_+(T, V)$, which stands for the probability distribution of T given that the last measurement of the input Z was positive, and $f_-(T, V)$, which stands for the probability distribution of T given that the last measurement of Z was negative. Therefore, $\Delta t f_+(T, V)$ is the probability that starting from a voltage $V(t)$ and given that $Z(t)$ was positive, threshold is reached between T and $T + \Delta t$ time units later. In turn, using the proper discretization for this case (see equation 5.1), the same

reasoning that previously led to equation 4.4 now leads to a set of two coupled equations:

$$f_+(T + \Delta t, V) = f_+(T, V + (\mu + \sigma)\Delta t)(1 - P_c) + f_-(T, V + (\mu - \sigma)\Delta t)P_c \quad (5.3)$$

$$f_-(T + \Delta t, V) = f_+(T, V + (\mu + \sigma)\Delta t)P_c + f_-(T, V + (\mu - \sigma)\Delta t)(1 - P_c). \quad (5.4)$$

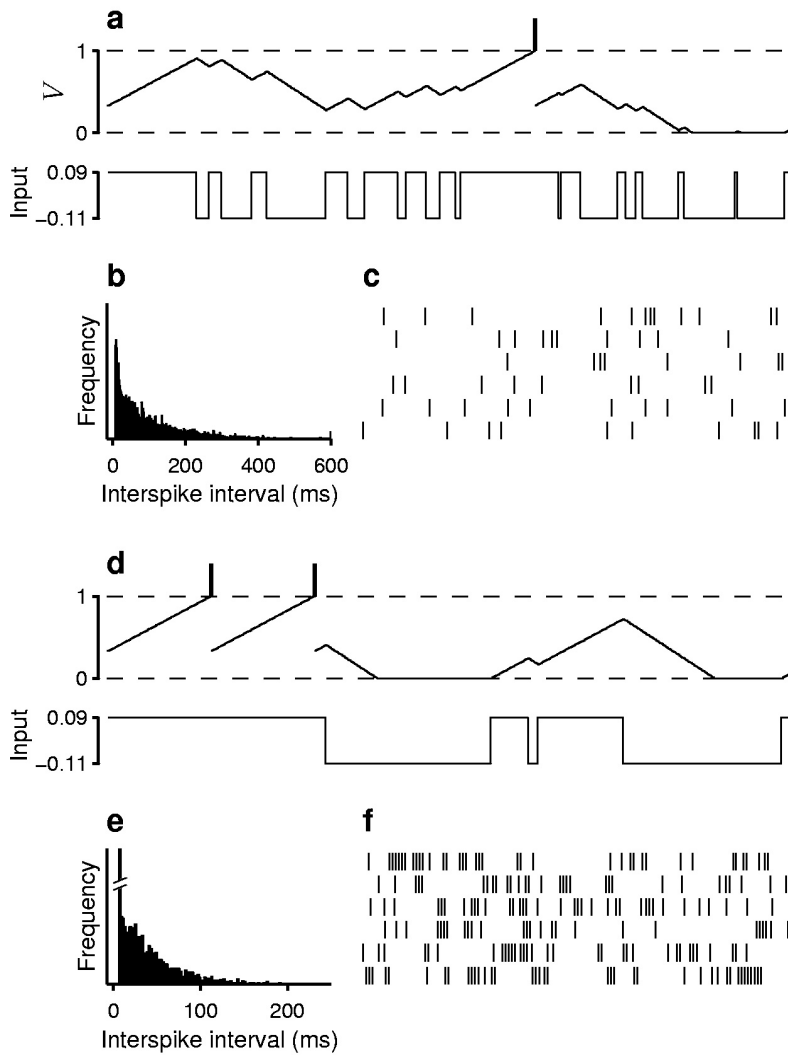
The first equation follows when $Z(t)$ is positive, so $Z(t + \Delta t)$ can either stay positive, with probability $1 - P_c$, or change to negative, with probability P_c ; similarly, the second equation means that when the current Z at time t is negative, at time $t + \Delta t$ it can either become positive, with probability P_c , or stay negative, with probability $1 - P_c$. At this point, one may proceed as in the case of uncorrelated noise: expand each term in a Taylor series, which in this case only needs to be of first order, substitute P_c for $\Delta t/2\tau_{corr}$, simplify terms, and take the limit $\Delta t \rightarrow 0$. The result is a pair of coupled differential equations for f_+ and f_- analogous to equation 4.5 when input samples are independent:

$$\begin{aligned} \frac{\partial f_+}{\partial T} &= -\frac{1}{2\tau_{corr}}(f_+ - f_-) + (\mu + \sigma)\frac{\partial f_+}{\partial V} \\ \frac{\partial f_-}{\partial T} &= \frac{1}{2\tau_{corr}}(f_+ - f_-) + (\mu - \sigma)\frac{\partial f_-}{\partial V}. \end{aligned} \quad (5.5)$$

Figure 4: *Facing page*. Responses of the nonleaky integrate-and-fire model driven by correlated, binary noise. The input switches signs randomly, but on average the same sign is maintained for $2\tau_{corr}$ time units. (a) Sample voltage and input timecourses. Traces represent 50 ms of simulation time, with $\Delta t = 0.1$ ms. The top trace shows the model neuron's voltage V and the spikes produced. The bottom trace shows the total input $\mu + Z\sigma$ at each time step, where Z may be either $+1$ or -1 . The input has a negative drift, and firing is irregular. Parameters in equation 5.1 were $\mu = -0.01$, $\sigma = 0.1$; the correlation time was $\tau_{corr} = 1$ ms. (b) Interspike interval histogram with $\langle T \rangle = 96$ ms and $CV_{ISI} = 1$. (c) Spike raster showing 6 seconds of continuous simulation time; each line represents 1 second. The same parameters were used in *a* through *c*. Panels *d* through *f* have the same formats as the corresponding panels above, except that $\tau_{corr} = 5$ ms; thus, changes in the sign of the input in *d* occur about five times less frequently than in *a*. Note different x -axes for the interspike interval histograms. In *e*, the y -axis is truncated; 48% of the interspike intervals fall in the bin centered at 7 ms. In this case, $\langle T \rangle = 27$ ms, $CV_{ISI} = 1.18$. The increase in correlation time causes a large increase in firing rate and a smaller but still considerable increase in variability.

These equations may be multiplied by T^q and integrated, as was done in the previous section. The two equations that result describe how the moments of T change with voltage. These equations are:

$$\begin{aligned}
 -q\langle T_+^{q-1} \rangle &= -\frac{1}{2\tau_{corr}} \left(\langle T_+^q \rangle - \langle T_-^q \rangle \right) + (\mu + \sigma) \frac{d\langle T_+^q \rangle}{dV} \\
 -q\langle T_-^{q-1} \rangle &= \frac{1}{2\tau_{corr}} \left(\langle T_+^q \rangle - \langle T_-^q \rangle \right) + (\mu - \sigma) \frac{d\langle T_-^q \rangle}{dV}.
 \end{aligned} \tag{5.6}$$



Notice that there are two sets of moments, not just one, because there are two conditional distributions, f_+ and f_- . We should point out that for the most part, $\langle T_+ \rangle$ is the crucial quantity. It corresponds to the average time required to reach threshold starting at voltage V and given that the last value of the current was positive; similarly, $\langle T_- \rangle$ is the expected time required to reach threshold starting at voltage V but given that the last value of Z was negative. However, notice that in a spike train a new excursion from reset to threshold is initiated immediately after each spike, and all spikes must be preceded by an increase in voltage. With one exception, this always corresponds to $Z > 0$, in which case the quantities of interest are $\langle T_+ \rangle$, $\langle T_+^2 \rangle$, and so on. The exception is when μ is positive and larger than σ ; in this case, V never decreases because the total input is always positive, and therefore threshold can be reached even after a negative value of Z .

For this same reason, the cases $\mu < \sigma$ and $\mu > \sigma$ will require different boundary conditions. When σ is larger than μ , the sign of the corresponding change in voltage is equal to the sign of Z (this is not true if μ is negative and $|\mu| > \sigma$, but then the voltage cannot increase and no spikes are ever produced, so we disregard this case). The first boundary condition is then

$$\frac{\partial f_-(T, 0)}{\partial V} = 0, \quad (5.7)$$

which corresponds to the presence of the barrier at $V = 0$. It involves the function f_- because the barrier can be reached only after a negative value of Z . Therefore, there is no corresponding condition for f_+ . Second,

$$f_+(T, V_\theta) = \delta(T). \quad (5.8)$$

This is the condition on the threshold, which can be reached only after a positive value of Z ; hence, the use of f_+ . In terms of the moments of T , these conditions become

$$\begin{aligned} \frac{d\langle T_-^q \rangle}{dV}(V = 0) &= 0 \\ \langle T_+^q \rangle(V = V_\theta) &= 0. \end{aligned} \quad (5.9)$$

When μ is positive and larger than σ , the change in voltage in one time step is always positive. In this case, the barrier is never reached, so there is no boundary condition at that point. Threshold, however, can be reached with either positive or negative Z values, so the two conditions are

$$\begin{aligned} f_+(T, V_\theta) &= \delta(T) \\ f_-(T, V_\theta) &= \delta(T), \end{aligned} \quad (5.10)$$

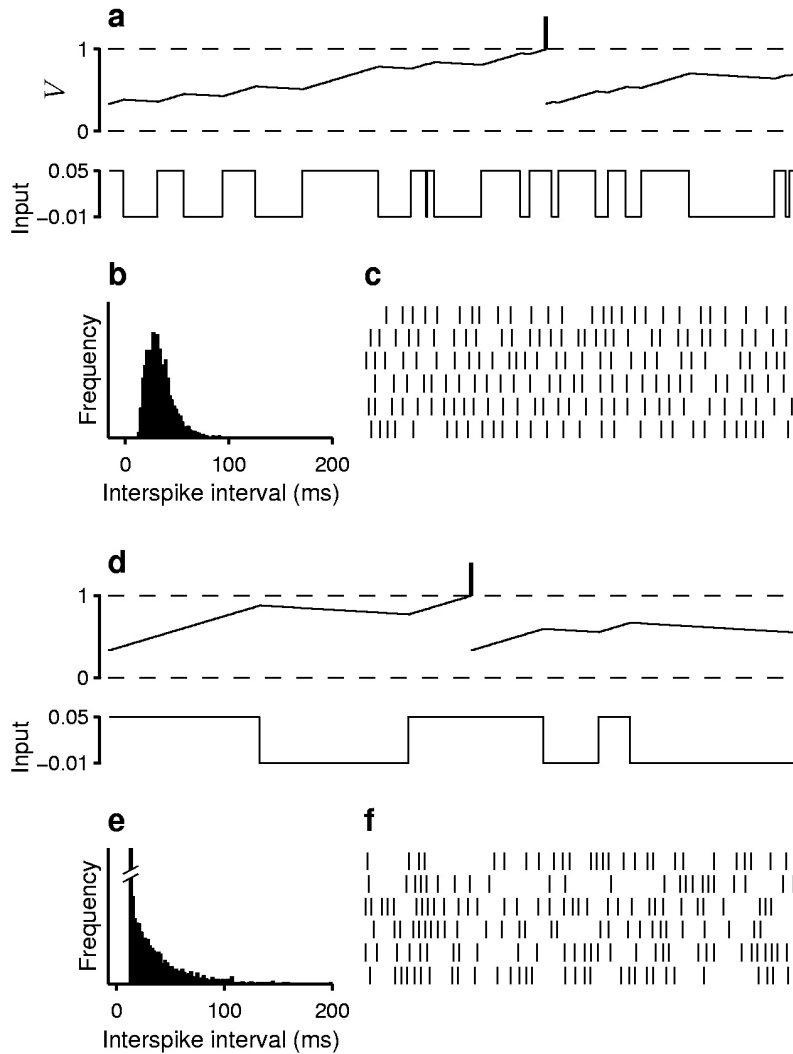


Figure 5: As in Figure 4, except that $\mu = 0.02$, $\sigma = 0.03$. The input has a strong positive drift, which gives rise to much more regular responses. (a–c) $\tau_{corr} = 1$ ms, $\langle T \rangle = 33$ ms, and $CV_{ISI} = 0.37$. (d–f) $\tau_{corr} = 5$ ms, $\langle T \rangle = 33$ ms, and $CV_{ISI} = 0.81$. (e) Twenty-eight percent of the interspike intervals fall in the bin centered at 13 ms, and the y -axis is truncated. In this case, the increase in correlation time does not affect the firing rate but produces a large increase in variability.

and for the moments of T , this gives

$$\begin{aligned}\langle T_+^q \rangle(V = V_\theta) &= 0 \\ \langle T_-^q \rangle(V = V_\theta) &= 0.\end{aligned}\quad (5.11)$$

5.2 Solutions for $\sigma \geq \mu$. Ordinary differential equations for the mean first passage time are obtained by setting $q = 1$ in equations 5.6. The solutions to these equations are

$$\begin{aligned}\langle T_+ \rangle(V) &= \phi_1^+(V_\theta) - \phi_1^+(V) \\ \phi_1^+(x) &= \frac{x}{\mu} + \tau_{corr}(c-1)^2 \exp(-\alpha x) \\ \langle T_- \rangle(V) &= \phi_1^+(V_\theta) + 2\tau_{corr}c - \frac{V}{\mu} - \tau_{corr}(c^2-1) \exp(-\alpha V),\end{aligned}\quad (5.12)$$

where we have defined

$$\begin{aligned}c &\equiv \frac{\sigma}{\mu} = \frac{\sigma_1}{\mu_0} \\ \alpha &\equiv \frac{1}{\mu\tau_{corr}(c^2-1)}.\end{aligned}\quad (5.13)$$

These expressions satisfy the boundary conditions 5.9 for the threshold and the barrier. Ordinary differential equations for the second moments of the first passage time are obtained by setting $q = 2$ in equations 5.6 and inserting the above expressions for $\langle T_+ \rangle$ and $\langle T_- \rangle$. The solutions to the second moment equations are

$$\begin{aligned}\langle T_+^2 \rangle(V) &= \phi_2^+(V_\theta) - \phi_2^+(V) \\ \phi_2^+(x) &= x \left(\frac{2\phi_1^+(V_\theta)}{\mu} + \frac{2\tau_{corr}c^2}{\mu} \right) - \frac{x^2}{\mu^2} \\ &\quad + 2\tau_{corr}(c-1)^2 \left(\phi_1^+(V_\theta) + \tau_{corr}(2c^2+4c+1) \right) \exp(-\alpha x) \\ &\quad + \frac{2\tau_{corr}(c-1)(c^2+1)}{\mu(c+1)} x \exp(-\alpha x) \\ \langle T_-^2 \rangle(V) &= \phi_2^+(V_\theta) + 4c\tau_{corr}\phi_1^+(V_\theta) + 4\tau_{corr}^2c^2(c+1) \\ &\quad - V \left(\frac{2\phi_1^+(V_\theta)}{\mu} + \frac{2\tau_{corr}c(c+2)}{\mu} \right) + \frac{V^2}{\mu^2} \\ &\quad - 2\tau_{corr}(c^2-1) \left(\phi_1^+(V_\theta) + \tau_{corr}(2c^2+2c+1) \right) \exp(-\alpha V) \\ &\quad - \frac{2\tau_{corr}(c^2+1)}{\mu} V \exp(-\alpha V).\end{aligned}\quad (5.14)$$

These also satisfy boundary conditions 5.9, with $q = 2$. As explained above, the relevant quantities in this case are $\langle T_+ \rangle$ and $\langle T_+^2 \rangle$, because threshold is always reached following a positive value of Z . Thus, $\langle T_+ \rangle$ should be equal to the mean first passage time calculated from simulated spike trains.

What is the behavior of these solutions as τ_{corr} increases? Consider the firing rate r of the model neuron under these conditions. As correlations become longer, the stretches of time during which input samples have the same sign also become longer (compare the lower traces in Figures 4a and 4d), although on average it is still true that positive and negative samples are equally likely. During a stretch of consecutive negative samples, the firing rate is zero, whereas during a long stretch of consecutive positive samples, it must be equal to

$$r_+ = \frac{\mu + \sigma}{V_\theta - V_{reset}}, \quad (5.15)$$

which is just the rate we would obtain if the total input were constant and equal to $\mu + \sigma$ (see equation 4.14). Therefore, the mean rate for large τ_{corr} should be approximately equal to one-half of r_+ . Indeed, in the above expression for $\langle T_+ \rangle$, one may expand the exponential in a Taylor series and take the limit $\tau_{corr} \rightarrow \infty$; the result is that, in the limit, the firing rate is equal to $r_+/2$.

On the other hand, longer correlation times give rise to longer stretches in which no spikes appear, that is, longer interspike intervals. Thus, in contrast to the mean, the variance in the interspike interval distribution should keep increasing. This can be seen from the above expression for $\langle T_+^2 \rangle$: again, expand the exponentials in Taylor series, but note that this time, the coefficient of the final term in V includes τ_{corr} , so $\langle T_+^2 \rangle$ will keep increasing with the correlation time. Because the CV_{ISI} is a function of $\langle T_+^2 \rangle / \langle T_+ \rangle^2$, the variability of the spike trains generated by the model will diverge as the correlation time increases.

Another interesting limit case is obtained when $\sigma = \mu$, or $c = 1$. Here, the total input is zero every time that Z equals -1 ; this means that half the time, V does not change, whereas the rest of the time, V changes by 2μ in each time step. On average, this gives a time to threshold $\langle T_+ \rangle$ equal to $(V_\theta - V_{reset})/\mu$, which is precisely the result from equation 5.12. Notice that this quantity does not depend on the correlation time. In contrast, the second moment $\langle T_+^2 \rangle$ does depend on τ_{corr} . For this case, $c = 1$, the expression for the CV_{ISI} is particularly simple:

$$\sqrt{\frac{2\mu\tau_{corr}}{V_\theta - V_{reset}}}. \quad (5.16)$$

Thus, again the variability diverges as τ_{corr} increases, but the mean rate does not.

5.3 Solutions for Zero Drift ($\mu = 0$). When the drift is exactly zero, the model neuron is driven by the zero-mean input only. Equations for the moments of the first passage time are obtained as above, using the proper values of q in equations 5.6, but $\mu = 0$ must also be set in these expressions. With these considerations, the solutions for the mean first passage time in the case of correlated noise with zero drift are

$$\begin{aligned}\langle T_+ \rangle(V) &= \psi_1^+(V_\theta) - \psi_1^+(V) \\ \psi_1^+(x) &= \frac{2x}{\sigma} + \frac{x^2}{2\tau_{corr}\sigma^2} \\ \langle T_- \rangle(V) &= \psi_1^+(V_\theta) + 2\tau_{corr} - \frac{V^2}{2\tau_{corr}\sigma^2}.\end{aligned}\quad (5.17)$$

Notice that these expressions can also be obtained from the solutions to the case $\sigma > \mu$ by expanding the exponentials in equations 5.12 in Taylor series, cancelling terms, and then taking the limit $\mu \rightarrow 0$.

For the second moment,

$$\begin{aligned}\langle T_+^2 \rangle(V) &= \psi_2^+(V_\theta) - \psi_2^+(V) \\ \psi_2^+(x) &= \frac{4x}{\sigma} (\tau_{corr} + \psi_1^+(V_\theta)) + \frac{x^2}{\tau_{corr}\sigma^2} (-\tau_{corr} + \psi_1^+(V_\theta)) \\ &\quad - \frac{2x^3}{3\tau_{corr}\sigma^3} - \frac{x^4}{12\tau_{corr}^2\sigma^4} \\ \langle T_-^2 \rangle(V) &= \psi_2^+(V_\theta) + 4\tau_{corr} (2\tau_{corr} + \psi_1^+(V_\theta)) \\ &\quad - \frac{V^2}{\tau_{corr}\sigma^2} (\tau_{corr} + \psi_1^+(V_\theta)) + \frac{V^4}{12\tau_{corr}^2\sigma^4}.\end{aligned}\quad (5.18)$$

The boundary conditions satisfied by these solutions are those given by equations 5.9, as in the previous case. Also, it is $\langle T_+ \rangle$ and $\langle T_+^2 \rangle$ that are important, because spikes are always triggered by positive values of the fluctuating input.

The asymptotic behavior of these solutions for increasing τ_{corr} is similar to that in the previous case. In the limit, the mean rate is again given by $r_+/2$ (with $\mu = 0$), and it is clear from the expression for ψ_2^+ that $\langle T_+^2 \rangle$ will diverge because of the leading term $4x\tau_{corr}/\sigma$.

5.4 Solutions for $\sigma < \mu$. When σ is smaller than μ , the same differential equations discussed above (equations 5.6 with the appropriate values of q) need to be solved, but the boundary conditions are different. In this case, equations 5.11 should be satisfied. The solutions for the first moment that

do so are

$$\begin{aligned}\langle T_+ \rangle(V) &= \frac{V_\theta - V}{\mu} + \tau_{corr} c(c-1) (1 - \exp(\alpha(V_\theta - V))) \\ \langle T_- \rangle(V) &= \frac{V_\theta - V}{\mu} + \tau_{corr} c(c+1) (1 - \exp(\alpha(V_\theta - V))).\end{aligned}\quad (5.19)$$

In contrast to the previous two situations, now threshold can be reached after a positive or a negative value of Z . Overall, these are equally probable, but the relative numbers of spikes triggered by $Z = +1$ and $Z = -1$ need not be, so determining the observed mean first passage time becomes more difficult. The following approximation works quite well.

Consider the case where τ_{corr} is large. The interspike interval during a long stretch of positive samples is still equal to $(V_\theta - V_{reset})/(\mu + \sigma)$, but spikes are also produced during a long stretch of negative samples, with an interspike interval equal to $(V_\theta - V_{reset})/(\mu - \sigma)$. This suggests that the number of excursions to threshold that start after $Z = +1$ during a given period of time should be proportional to $\mu + \sigma$, whereas those that start after $Z = -1$ in the same period should be proportional to $\mu - \sigma$. Using these quantities as weighting coefficients for $\langle T_+ \rangle$ and $\langle T_- \rangle$ gives

$$\langle T_A \rangle(V) = \frac{(\mu + \sigma)\langle T_+ \rangle + (\mu - \sigma)\langle T_- \rangle}{2\mu} = \frac{V_\theta - V}{\mu},\quad (5.20)$$

where the second equality is obtained by using equations 5.19. This average should approximate the mean time between spikes produced by the model. According to this derivation, when $\sigma < \mu$, the mean first passage time should be constant as a function of the correlation time (as was found when $c = 1$).

Obtaining an expression for the second moment of the first passage time requires a similar averaging procedure. First, using equations 5.19 on the left-hand side, solutions to equations 5.6 for $q = 2$ are found; these are

$$\begin{aligned}\langle T_+^2 \rangle(V) &= \varphi_2^+(V_\theta) - \varphi_2^+(V) \\ \langle T_-^2 \rangle(V) &= \varphi_2^-(V_\theta) - \varphi_2^-(V),\end{aligned}\quad (5.21)$$

where

$$\begin{aligned}\varphi_2^\pm(x) &= \frac{2}{\mu} \left(\frac{V_\theta}{\mu} + 2\tau_{corr}c^2 \mp \tau_{corr}c \right) x - \frac{x^2}{\mu^2} \\ &\quad + 2\tau_{corr}^2c^2 (3c^2 \mp 2c - 1) \exp(\alpha(V_\theta - x)) \\ &\quad - \left(\frac{2\tau_{corr}}{\mu} \frac{c(c^2 + 1)}{c \pm 1} \right) (V_\theta - x) \exp(\alpha(V_\theta - x)).\end{aligned}\quad (5.22)$$

These solutions satisfy boundary conditions 5.11. Second, again considering that the relative frequencies of spikes triggered by $Z = +1$ and $Z = -1$ should be proportional to $\mu + \sigma$ and $\mu - \sigma$, respectively, one obtains

$$\begin{aligned} \langle T_A^2 \rangle(V) &= \frac{(\mu + \sigma)\langle T_+^2 \rangle + (\mu - \sigma)\langle T_-^2 \rangle}{2\mu} \\ &= \left(\frac{V_\theta - V}{\mu}\right)^2 + 2\tau_{corr}c^2\left(\frac{V_\theta - V}{\mu}\right) \\ &\quad + 2\tau_{corr}^2c^2(c^2 - 1)(1 - \exp(\alpha(V_\theta - V))). \end{aligned} \quad (5.23)$$

Recall that the quantities α and c are defined in equation 5.13 and apply to all solutions.

In this case, the asymptotic behavior of the solutions as functions of τ_{corr} is different from the previous cases. As noted above, the mean first passage time is independent of τ_{corr} so, as in the case $\sigma \geq \mu$, it remains finite as τ_{corr} increases. The variability, however, does not diverge in this case, as it does when $\sigma < \mu$. In the limit when $\tau_{corr} \rightarrow \infty$, the second moment tends to a finite value; this is not obvious from equation 5.23, but expanding the exponentials, one finds that all terms with τ_{corr} in the numerator cancel out. Intuitively, this makes sense: as the correlation time increases, the value of most interspike intervals tends to be either $(V_\theta - V_{reset})/(\mu - \sigma)$ or $(V_\theta - V_{reset})/(\mu + \sigma)$, so the variance in the interspike interval distribution tends to a constant. The CV_{ISI} in this limit case is also given by a simple expression, which is

$$\frac{c}{\sqrt{1 - c^2}}. \quad (5.24)$$

Plots of the solutions just presented are shown in Figures 6 and 7. The format of these figures is the same as in Figures 2 and 3: dots and continuous lines correspond to computer simulations and analytic solutions, respectively. Here, however, three sets of curves and dots appear in each panel; these correspond to τ_{corr} equal to 1, 3, and 10 ms, where higher correlation times give rise to higher values of the mean rate and CV_{ISI} . As in the case of independent input samples, their agreement is excellent. It is evident from these figures that the correlation time increases both the firing rate and the variability of the responses for any fixed combination of μ and σ .

Two important points should be noted. First, the relative effect on the mean firing rate is much stronger when σ is large compared to μ . This is most evident in Figure 7b (top row), where the effect of τ_{corr} is enormous when μ is zero or negative and becomes negligible as μ becomes comparable to σ . This is also clear in Figure 6c where, in agreement with equation 5.20, the firing rate remains constant for $\sigma < \mu$ and becomes more sensitive to τ_{corr} as σ increases. The higher sensitivity when σ is large is not at all surprising because correlations do not alter the drift. Hence, when the neuron

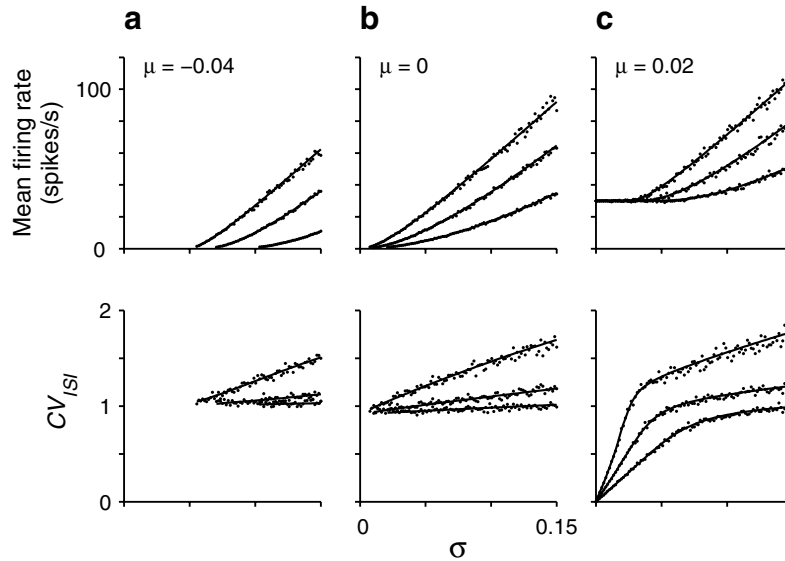


Figure 6: Mean firing rate and coefficient of variation for the nonleaky integrate-and-fire neuron driven by correlated noise. Continuous lines are analytic expressions, and dots are results from computer simulations using a binary input. For each simulation data point, $\langle T \rangle$ and $\langle T^2 \rangle$ were calculated from spike trains containing 2,000 spikes (same in following figures). Results are shown as functions of σ for the three values of μ indicated in the top-left corner of each panel. The three curves in each graph correspond to $\tau_{corr} = 1$ (lower curves), $\tau_{corr} = 3$ (middle curves), and $\tau_{corr} = 10$ ms (upper curves). (a, c) The continuous lines were obtained from equations 5.12 through 5.14, which apply to $\mu < \sigma$, except in the initial part of c, where $\mu > \sigma$ and equations 5.20 and 5.23 were used. (b) The continuous lines were obtained from equations 5.17 and 5.18. Both firing rate and variability increase with correlation time.

is being primarily driven by drift, the change in rate caused by correlations is proportionally small.

The second key point is that as the correlation time is increased, the effect on the firing rate saturates, but the effect on variability may not. For instance, in Figures 6a through 6c (top row), the difference between the lower two and the upper two rate curves is about the same, although the latter corresponds to a much larger increase in correlation time. In contrast, the CV_{ISI} plots in the same figure do show larger differences between CV_{ISI} traces for larger changes in τ_{corr} .

Figure 8 illustrates these points more clearly. Here, the mean rate and the CV_{ISI} are plotted as functions of the correlation time τ_{corr} for various combinations of μ and σ . Only analytic results are shown here, but these

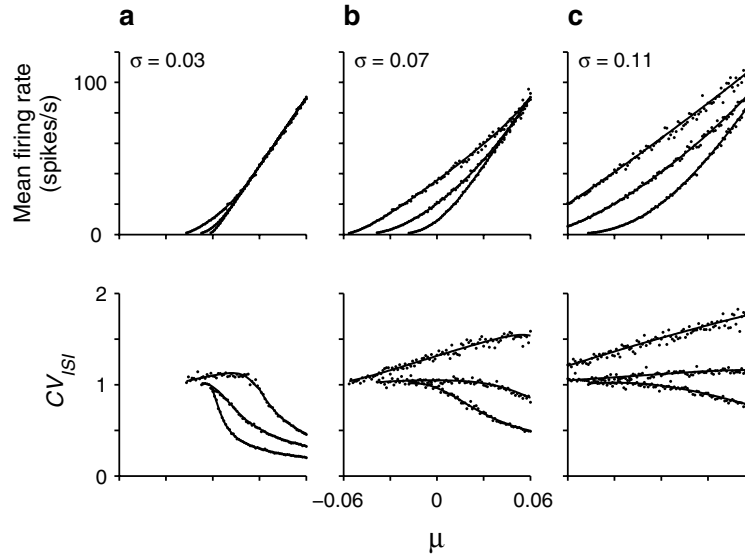


Figure 7: As in Figure 6, but the mean firing rate and coefficient of variation are plotted as functions of μ for the three values of σ indicated. The three curves in each graph again correspond to $\tau_{corr} = 1$ (lower curves), $\tau_{corr} = 3$ (middle curves), and $\tau_{corr} = 10$ ms (upper curves). All continuous lines were obtained from equations 5.12 through 5.14 ($\mu < \sigma$), except for the last part of *a*, where equations 5.20 and 5.23 were used ($\mu > \sigma$).

were confirmed by additional simulations. First, notice the behavior of the firing rate: it increases as a function of τ_{corr} up to a certain point, where it saturates. The net increase in rate is larger for higher values of σ and smaller for higher values of μ . On the other hand, the variability shows different asymptotic behaviors in the cases $\sigma > \mu$ and $\sigma < \mu$. In the former, the CV_{ISI} always keeps rising with longer correlation times; in the latter, it saturates (see the thickest trace in Figure 8b, bottom). This saturation value is in accordance with equation 5.24, which, for the parameter values used in the figure, predicts a limit CV_{ISI} of 0.98.

In the following sections, similar analyses are presented for the integrate-and-fire model with leak. Although the quantitative details differ somewhat, the main conclusions just discussed remain true for this model too.

6 The Leaky Integrate-and-Fire Neuron

The integrate-and-fire model with leak (Tuckwell, 1988; Troyer & Miller, 1997; Salinas & Sejnowski, 2000; Dayan & Abbott, 2001) provides a more accurate description of the voltage dynamics of a neuron while still being

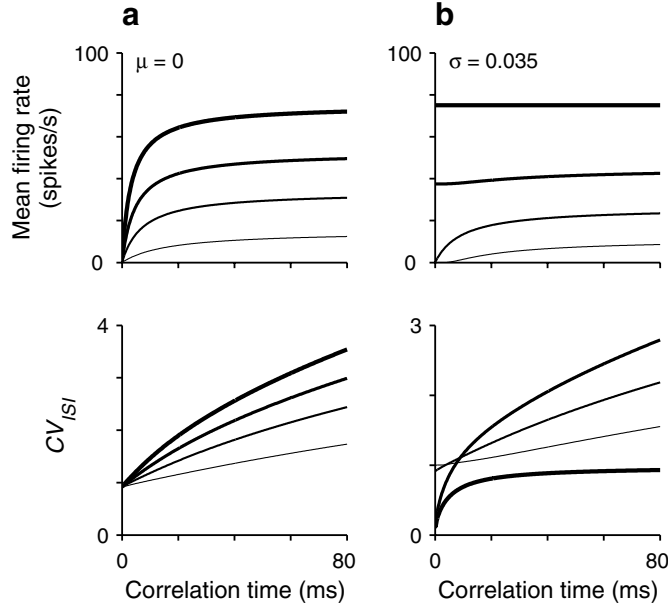


Figure 8: Responses of the nonleaky integrate-and-fire neuron as functions of the correlation time τ_{corr} . Only analytic results are shown. Plots on the top and bottom rows show the mean firing rate and CV_{ISI} , respectively. (a) The four curves shown in each plot correspond to four values of σ : 0.02, 0.045, 0.07, and 0.1, with thicker lines corresponding to higher values. For all these curves, $\mu = 0$, as indicated. (b) The four curves shown in each plot correspond to four values of μ : -0.02 , 0, 0.025, and 0.05, with thicker lines corresponding to higher values. For all these curves, $\sigma = 0.035$, as indicated. As the correlation time increases, the firing rate tends to an asymptotic value. In contrast, the CV_{ISI} diverges always, except when $\mu > \sigma$; this case corresponds to the thickest line in *b*.

quite simple. When driven by a stochastic input, the evolution equation for the voltage may be written as follows,

$$\tau \frac{dV}{dt} = -V + \mu_0 + X(t), \quad (6.1)$$

where the input terms are the same as before. The key difference is the $-V$ term. Again, a spike is produced when V exceeds the threshold V_θ , after which V is reset to V_{reset} . Note, however, that in this case, there is no barrier. This equation can be further simplified by defining

$$v \equiv V - \mu_0, \quad (6.2)$$

in which case only the fluctuating component of the input (with zero mean) appears in the equation

$$\tau \frac{dv}{dt} = -v + X(t). \quad (6.3)$$

The threshold and reset values need to be transformed accordingly:

$$\begin{aligned} v_\theta &\equiv V_\theta - \mu_0 \\ v_{reset} &\equiv V_{reset} - \mu_0. \end{aligned} \quad (6.4)$$

It is easier to solve equations using v , but when the effects of μ_0 , σ_1 , and τ_{corr} are discussed, V is more convenient. These equations will be used to shift between V and v representations.

It is in the form of equation 6.3 that the leaky integrate-and-fire model becomes identical to the Ornstein-Uhlenbeck process (Uhlenbeck & Ornstein, 1930; Ricciardi, 1977, 1995; Shinomoto et al., 1999). Notice that in this model, v is driven toward X ; if X were to remain constant at $X = X_0$, v would tend exponentially toward this value with a time constant τ . If X_0 were above threshold, the interspike interval would be constant and equal to

$$T = \tau \log \left(\frac{X_0 - v_{reset}}{X_0 - v_\theta} \right), \quad (6.5)$$

which results from integrating equation 6.3. This is a well-known result. Note that spikes may be produced even if X_0 is zero or negative, as long as it is above threshold. With binary inputs, the drive X switches randomly between two values.

Although this model remains an extreme simplification of a real neuron, its analytic treatment is more complicated than for the nonleaky model. Considerable work has been devoted to solving the first passage time problem when the model is driven by uncorrelated gaussian noise (Thomas, 1975; Ricciardi, 1977, 1995; Ricciardi & Sacerdote, 1979; Ricciardi & Sato, 1988). Although closed-form expressions for the moments of T in this case are not known, solutions in terms of series expansions have been found; these are well described by Shinomoto et al. (1999) and will not be considered any further here.

In the remainder of the article, we investigate the responses of the leaky integrate-and-fire model when X represents correlated binary noise, as was done for the nonleaky model. As before, we are interested in the time T that it takes for v to go from reset to threshold—the first passage time, or interspike interval.

6.1 Equations for the Moments of T of the Leaky Neuron Driven by Correlated Noise. For a correlated random current, the discretized version of equation 6.3 can be written as

$$v(t + \Delta t) = v(t) + \left(-\frac{v(t)}{\tau} + \sigma Z \right) \Delta t, \quad (6.6)$$

where $Z = \pm 1$ and Z has an exponential correlation function, as discussed before. Again, the statistics of T are described by the two probability density functions $f_+(T, v)$ and $f_-(T, v)$, where $f_+(T, v)\Delta t$ and $f_-(T, v)\Delta t$ stand for the probability that starting from a voltage v , threshold is reached between T and $T + \Delta t$ time units later; f_+ is conditional on the last measurement of Z being positive, and f_- is conditional on the last measurement of Z being negative. The derivation of these functions proceeds in exactly the same way as for the nonleaky model; the key is that equation 6.6 has the same form as equation 5.1, except that the $-v/\tau$ term occupies the place of μ . Because it is f_+ and f_- that are expanded as functions of their arguments, all the corresponding expressions can be found by exchanging $-v/\tau$ for μ . Starting with equation 5.4, this leads to a set of two coupled differential equations for the moments of T analogous to equations 5.6:

$$\begin{aligned} -q\langle T_+^{q-1} \rangle &= -\frac{1}{2\tau_{corr}} \left(\langle T_+^q \rangle - \langle T_-^q \rangle \right) + \frac{\sigma_1 - v}{\tau} \frac{d\langle T_+^q \rangle}{dv} \\ -q\langle T_-^{q-1} \rangle &= \frac{1}{2\tau_{corr}} \left(\langle T_+^q \rangle - \langle T_-^q \rangle \right) - \frac{\sigma_1 + v}{\tau} \frac{d\langle T_-^q \rangle}{dv}. \end{aligned} \quad (6.7)$$

Notice that here we use the original variable σ_1 rather than the scaled one $\sigma = \sigma_1/\tau$ (see equation 5.2).

In addition to these equations, boundary conditions are required to determine the solution. The threshold mechanism is still the same, so applying equation 5.8, we obtain

$$\langle T_+^q \rangle(v = v_\theta) = 0, \quad (6.8)$$

which means that a spike must be emitted with no delay when v reaches threshold after a positive fluctuation. Note also that the model can produce spikes only when σ_1 is larger than the threshold value, because the maximum value that v may attain is precisely σ_1 .

For the second boundary condition, there are two possibilities. First, consider the case $v_\theta < -\sigma_1$. Since the input is binary, the voltage is driven toward either σ_1 or $-\sigma_1$, depending on the value of Z . If the threshold is lower than $-\sigma_1$, then both $Z = +1$ and $Z = -1$ may trigger a spike. Therefore,

$$\langle T_-^q \rangle(v = v_\theta) = 0, \quad (6.9)$$

which means that a spike must also be emitted without delay when v reaches threshold after a negative fluctuation. In the second case, $\sigma_1 > v_\theta > -\sigma_1$; when $Z = -1$, the voltage tends to go below threshold, so a spike can only be triggered by $Z = +1$. What is the second boundary condition then? This case is much more subtle. To obtain the new condition, first rewrite the bottom expression in equations 6.7 as follows:

$$\frac{d\langle T_-^q \rangle}{dv} = \frac{\tau}{\sigma_1 + v} \left(q \langle T_-^{q-1} \rangle + \frac{1}{2\tau_{corr}} (\langle T_+^q \rangle - \langle T_-^q \rangle) \right). \quad (6.10)$$

Now notice that the derivative has a singularity at $v = -\sigma_1$. However, the excursion toward threshold may start at any value below it, including $-\sigma_1$, so for any q , the derivative on the left side should be a continuous function of v . In other words, the derivative should not be allowed to diverge. Continuity requires that the limits obtained by approaching from the left and right be the same, that is,

$$\lim_{v \rightarrow -\sigma_1^+} \frac{d\langle T_-^q \rangle}{dv} = \lim_{v \rightarrow -\sigma_1^-} \frac{d\langle T_-^q \rangle}{dv}. \quad (6.11)$$

Expanding $\langle T_+^q \rangle$ and $\langle T_-^q \rangle$ in first-order Taylor series around σ_1 and using the above expression leads to the sought boundary condition,

$$\langle T_-^q \rangle(v = -\sigma_1) = \langle T_+^q \rangle(v = -\sigma_1) + 2\tau_{corr}q \langle T_-^{q-1} \rangle(v = -\sigma_1). \quad (6.12)$$

Setting $q = 1$ in equations 6.7, we obtain the differential equations for the mean first passage time,

$$\begin{aligned} -1 &= -\frac{1}{2\tau_{corr}} (\langle T_+ \rangle - \langle T_- \rangle) + \frac{\sigma_1 - v}{\tau} \frac{d\langle T_+ \rangle}{dv} \\ -1 &= \frac{1}{2\tau_{corr}} (\langle T_+ \rangle - \langle T_- \rangle) - \frac{\sigma_1 + v}{\tau} \frac{d\langle T_- \rangle}{dv}, \end{aligned} \quad (6.13)$$

with boundary conditions

$$\begin{aligned} \langle T_+ \rangle(v = v_\theta) &= 0 \\ \langle T_- \rangle(v = -\sigma_1) &= \langle T_+ \rangle(v = -\sigma_1) + 2\tau_{corr}. \end{aligned} \quad (6.14)$$

In this case, the second boundary condition has an intuitive explanation. Suppose a spike has just been produced—this necessarily requires $Z = +1$ —

and the voltage is reset to $v_{reset} = -\sigma_1$. Now suppose that in the next time step, $Z = -1$, so the expected time until the next spike is $\langle T_- \rangle$. The voltage will not change until Z switches back to $+1$, because $Z = -1$ drives it precisely toward $-\sigma_1$. The moment Z becomes positive, the expected time to reach threshold becomes $\langle T_+ \rangle$ by definition. Therefore, the expected time to reach threshold starting from $Z = -1$ is equal to the expected time starting from $Z = +1$ plus the time one must wait for Z to switch back to $+1$, which is $2\tau_{corr}$; that is what the boundary condition says. This happens only at $v = -\sigma_1$ because it is only at that point that v stays constant during the wait.

Setting $q = 2$, we obtain the differential equations for the second moment of T ,

$$\begin{aligned} -2\langle T_+ \rangle &= -\frac{1}{2\tau_{corr}} \left(\langle T_+^2 \rangle - \langle T_-^2 \rangle \right) + \frac{\sigma_1 - v}{\tau} \frac{d\langle T_+^2 \rangle}{dv} \\ -2\langle T_- \rangle &= \frac{1}{2\tau_{corr}} \left(\langle T_+^2 \rangle - \langle T_-^2 \rangle \right) - \frac{\sigma_1 + v}{\tau} \frac{d\langle T_-^2 \rangle}{dv}, \end{aligned} \tag{6.15}$$

with boundary conditions

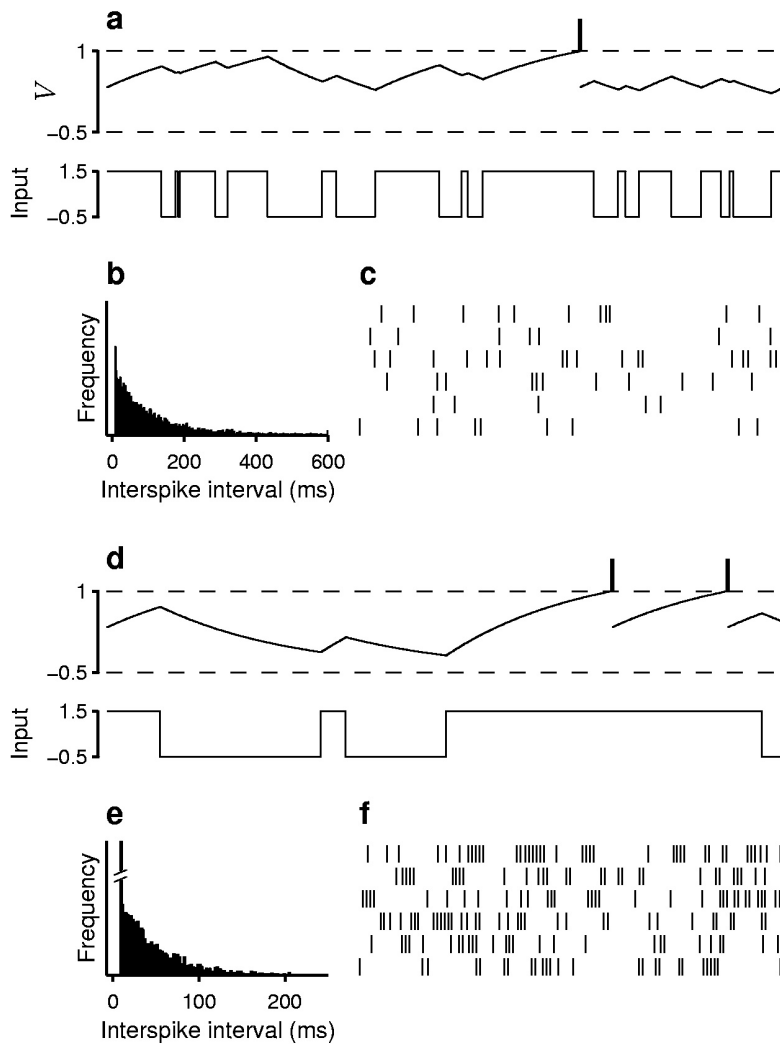
$$\begin{aligned} \langle T_+^2 \rangle(v = v_\theta) &= 0 \\ \langle T_-^2 \rangle(v = -\sigma_1) &= \langle T_+^2 \rangle(v = -\sigma_1) + 4\tau_{corr}\langle T_+ \rangle(v = -\sigma_1) + 8\tau_{corr}^2. \end{aligned} \tag{6.16}$$

Figure 9 shows voltage traces and spikes produced by the model with leak driven by a correlated binary input. The responses of the leaky integrator here are similar to those of the nonleaky model shown on Figure 4, but note that the voltage traces are now composed of piecewise exponential curves. In Figure 9, the neuron can spike only when Z is positive. In Figures 9a through 9c, the correlation time is $\tau_{corr} = 1$ ms, and on average the input changes sign every 2 ms (see Figure 9a, lower trace). When τ_{corr} is increased to 5 ms, the changes in sign occur approximately every 10 ms (see Figure 9d, lower trace), producing a large increase in mean firing rate and a smaller increase in CV_{ISI} . As with the nonleaky model, long correlation times generate many interspike intervals of minimum length, which in this case is 8.5 ms. For the leaky integrator, this minimum separation between spikes is equal to $\tau \log((\sigma_1 - v_{reset})/(\sigma_1 - v_\theta))$, which is just equation 6.5 with σ_1 instead of X_0 .

Analytic solutions for the mean firing rate and the CV_{ISI} of the leaky model driven by correlated noise can be obtained under some circumstances. These are derived below.

6.2 Solutions for $v_\theta > -\sigma_1$. First, consider the mean of T . Solutions in a closed form are not evident, but series expansions can be used. It may be verified by direct substitution that the following expressions satisfy differential equations 6.13 and their corresponding boundary conditions 6.14,

$$\begin{aligned} \langle T_+ \rangle &= \sum_{j=1} a_j \left((v_\theta + \sigma_1)^j - (v + \sigma_1)^j \right) \\ \langle T_- \rangle &= 2\tau_{corr} + \sum_{j=1} a_j (v_\theta + \sigma_1)^j - \sum_{j=1} b_j (v + \sigma_1)^j, \end{aligned} \quad (6.17)$$



where the coefficients a and b are given by the following recurrence relations,

$$\begin{aligned} a_1 &= \frac{\tau}{\sigma_1} \\ a_{j+1} &= \frac{a_j}{\sigma_1} \frac{j}{j+1} \frac{\tau + j\tau_{corr}}{\tau + 2j\tau_{corr}} \\ b_j &= a_j \frac{\tau}{\tau + 2j\tau_{corr}}. \end{aligned} \quad (6.18)$$

One of the limitations of series solutions is that they are valid only within a restricted range, known as the radius of convergence ρ . This radius can be found, for instance, by d'Alambert's ratio test,

$$\lim_{k \rightarrow \infty} \left| \frac{S_{k+1}}{S_k} \right| = \rho, \quad (6.19)$$

where S_k represents term k of the series (Jeffrey, 1995). The series converges for $\rho < 1$ and diverges for $\rho > 1$. Applying this test to the series

$$\sum_{j=1}^{\infty} a_j (v + \sigma_1)^j, \quad (6.20)$$

we find two conditions for convergence:

$$\begin{aligned} v &< \sigma_1, & \text{for } v > 0 \\ |v| &< 3\sigma_1, & \text{for } v < -\sigma_1. \end{aligned} \quad (6.21)$$

Note from equations 6.17 that these constraints must be satisfied for both $v = v_{reset}$ and $v = v_\theta$, but in practice the limitation is on v_{reset} . The first

Figure 9: *Facing page*. Responses of the leaky integrate-and-fire model driven by correlated, binary noise. Same format as in Figure 4. (a) Sample voltage and input timecourses. Note that the original variable V (and not v) is shown. Traces represent 50 ms of simulation time. The bottom trace shows the total input $\mu_0 + Z\sigma_1$ at each time step, where Z may be either +1 or -1. Parameters in equation 6.6 were $\mu_0 = 0.5$, $\sigma_1 = 1$, $\tau = 10$ ms; the correlation time was $\tau_{corr} = 1$ ms. (b) Interspike interval histogram, with $\langle T \rangle = 103$ ms and $CV_{ISI} = 0.94$. (c) Spike raster showing 6 seconds of continuous simulation time; each line represents 1 second. The same parameters were used in a through c . Panels d through f have the same formats as the corresponding panels above, except that $\tau_{corr} = 5$ ms. In e , the y-axis is truncated; 43% of the interspike intervals fall in the bin centered at 8 ms. In this case, $\langle T \rangle = 31$ ms, $CV_{ISI} = 1.15$. As in the model without leak, the increase in correlation time causes a large increase in firing rate and a smaller but still considerable increase in variability.

condition is always satisfied because the maximum value that the voltage can reach is σ_1 ; the second one means that the reset value cannot be set too negative (below $-3\sigma_1$). As will be discussed shortly, equations 6.17 and 6.18 provide an analytic solution that is valid within a fairly large range of parameters.

Now consider the second moment of T . The following series satisfy equations 6.15 with boundary conditions 6.16,

$$\begin{aligned}\langle T_+^2 \rangle &= \sum_{j=1} c_j \left((v_\theta + \sigma_1)^j - (v + \sigma_1)^j \right) \\ \langle T_-^2 \rangle &= 8\tau_{corr}^2 + 4\tau_{corr} \langle T_+ \rangle (v = -\sigma_1) + \sum_{j=1} c_j (v_\theta + \sigma_1)^j - \sum_{j=1} d_j (v + \sigma_1)^j, \quad (6.22)\end{aligned}$$

where the coefficients c and d are given by

$$\begin{aligned}c_1 &= \frac{2\tau}{\sigma_1} (\tau_{corr} + \langle T_+ \rangle (v = -\sigma_1)) \\ c_{j+1} &= \frac{1}{\sigma_1} \left[c_j \left(\frac{j}{j+1} \right) \frac{\tau + j\tau_{corr}}{\tau + 2j\tau_{corr}} - a_j \frac{\tau}{j+1} \left(1 + \left(\frac{\tau}{\tau + 2j\tau_{corr}} \right)^2 \right) \right] \\ d_j &= (c_j + 4\tau_{corr}b_j) \frac{\tau}{\tau + 2j\tau_{corr}}. \quad (6.23)\end{aligned}$$

These series solutions are obviously less transparent than the closed-form solutions found for the model without leak. However, a couple of interesting observations can be made. First, notice the behavior of $\langle T_+ \rangle$ as τ_{corr} tends to infinity: all the coefficients a become independent of τ_{corr} and remain finite. This means that $\langle T_+ \rangle$ saturates as a function of τ_{corr} . On the other hand, as expected, $\langle T_- \rangle$ tends to infinity, because of the leading term $2\tau_{corr}$ in equation 6.17. In contrast to the firing rate, the variability of the evoked spike trains does not saturate. Again, the reason is that as τ_{corr} increases, longer stretches of time are found during which no spikes are produced; these are the times during which $Z = -1$. The divergence of the CV_{ISI} is also apparent from the equations above: note that c_1 contains a term proportional to τ_{corr} . This and the fact that the rate saturates make the CV_{ISI} grow without bound.

6.3 Solutions for $v_\theta < -\sigma_1$. When v_θ is below $-\sigma_1$, the neuron can fire even if $Z = -1$, so boundary conditions 6.8 and 6.9 should be used. Solutions in terms of series expansions can be obtained in this case too. For the first moment of T , these have the form

$$\begin{aligned}\langle T_+ \rangle &= \sum_{j=1} a_j (v_\theta - v)^j \\ \langle T_- \rangle &= \sum_{j=1} b_j (v_\theta - v)^j. \quad (6.24)\end{aligned}$$

Unfortunately, these solutions turn out to be of little use because they converge for a very limited range of parameters. When they do converge, the firing rate is typically very high, at which point the difference between $\langle T_+ \rangle$ and $\langle T_- \rangle$ is minimal. The solutions for the second moment of T have the same problem. Therefore, these expressions will be omitted, along with the corresponding recurrence relations for this case.

From the simulations, we have observed that when $v_\theta < -\sigma_1$, the input fluctuations have a minimal impact on the mean firing rate. In this case, the mean interspike interval $\langle T \rangle$ is well approximated by the interval expected just from the average drive, which is zero (or μ_0 in the V representation)—that is,

$$\langle T \rangle \approx \tau \log \left(\frac{v_{reset}}{v_\theta} \right), \quad (6.25)$$

which is equation 6.5 with $X_0 = 0$.

Figures 10 and 11 plot the responses of the model with leak for various combinations of μ_0 and σ_1 , using the same formats of Figures 6 and 7. Again the three sets of curves correspond to τ_{corr} equal to 1, 3, and 10 ms, with longer correlation times producing higher values of the mean rate and CV_{ISI} . In general, these figures show the same trends found for the model without leak: correlations increase both the firing rate and the variability of the responses for almost any fixed combination of μ and σ . The only exception occurs near the point $v_\theta = -\sigma_1$, which marks the transition between the two types of solution. Right below this point, the rate drops slightly as the correlation time increases. This can be seen in Figures 11a and 11b, where the transitions occur at $\mu_0 = 1.2$ and $\mu_0 = 1.5$, respectively. Other aspects of the responses are also slightly different for the two models, but the same kinds of regimes can be observed. For instance, compare Figures 6c and 10c; the rate in the leaky model does not stay constant for small values of σ , but the rise in CV_{ISI} is still quite steep. Also, in Figure 11, the firing rate is zero when $\mu_0 + \sigma_1$ is less than 1 (which is the threshold for V), so when the rates are low, the curves are clearly different. But notice how in Figure 11a the CV_{ISI} decreases for large values of μ_0 . In this regime, the variability saturates, as for the model without leak, because regardless of τ_{corr} there is a minimum firing rate.

The responses of the leaky integrate-and-fire neuron as functions of τ_{corr} are plotted in Figure 12. Series solutions were used in all cases except for the combination $\sigma_1 = 0.3$, $\mu_0 = 1.31$, for which simulation results are shown (dots). This is the case in which spikes can be produced after positive or negative Z and where the CV_{ISI} does not diverge. Note the overall similarity between the curves in Figures 12 and 8.

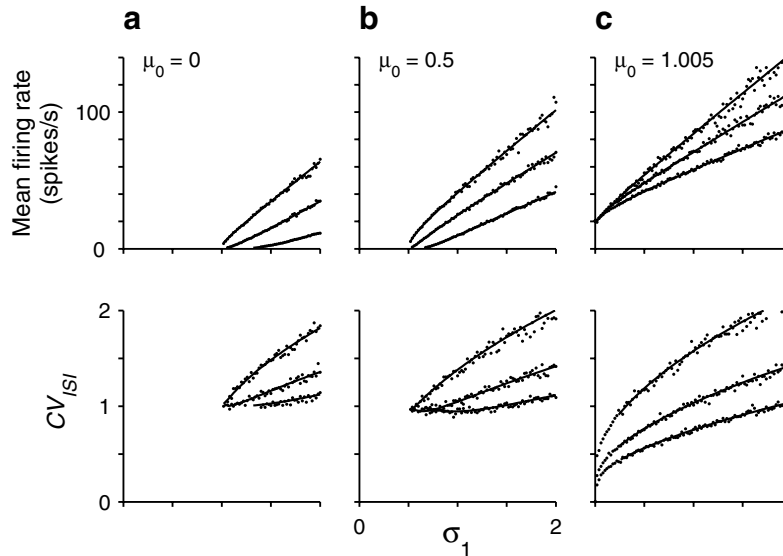


Figure 10: Mean firing rate and coefficient of variation for the leaky integrate-and-fire neuron driven by correlated noise. Continuous lines are analytic expressions, and dots are results from computer simulations using a binary input. Results are shown as functions of σ_1 for the three values of μ_0 indicated in the top-left corner of each panel. As in Figures 6 and 7, the three curves in each graph correspond to $\tau_{corr} = 1$ (lower curves), $\tau_{corr} = 3$ (middle curves), and $\tau_{corr} = 10$ ms (upper curves). The continuous lines were obtained from equations 6.17 and 6.22, which apply to $|v_{reset}| < 3\sigma_1$. This condition is not satisfied in c for σ_1 below 0.23, so the lines start above that value. Both firing rate and variability increase with correlation time.

7 Discussion

We have analyzed two simple integrate-and-fire model neurons whose responses are driven by a temporally correlated, stochastic input. Assuming that the input samples are binary and given their mean, variance, and correlation time, we were able to find analytic solutions for the first two moments of T , which is the time that it takes for the voltage to go from the starting value to threshold, at which point a spike is produced. We found that when other parameters were kept fixed, the correlation time tended to increase both the mean firing rate of the model neurons (the inverse of T) and the variability of the output spike trains, but the effects on these quantities differed in some respects. As the correlation time increased from zero to infinity, the firing rates always approached a finite limit value. In contrast, the CV_{ISI} approached a finite limit only when the input mean (or drift) was

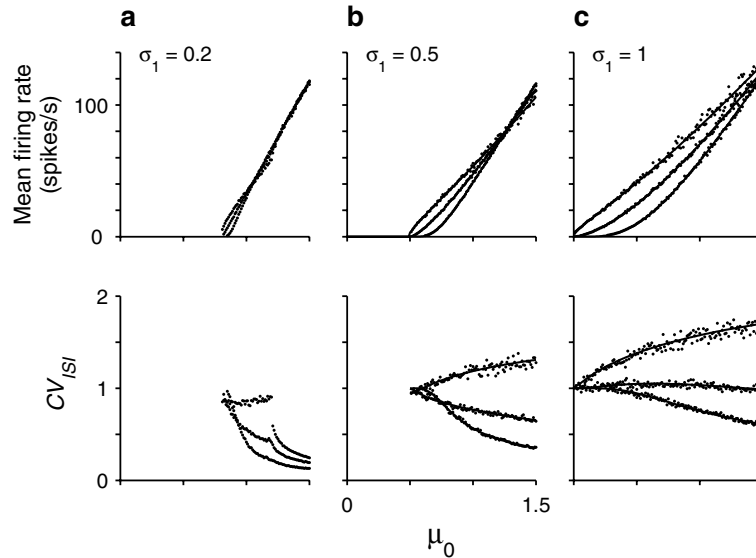


Figure 11: As in Figure 7, but the mean firing rate and coefficient of variation are plotted as functions of μ_0 for the three values of σ_1 indicated. The three curves in each graph again correspond to $\tau_{corr} = 1$ (lower curves), $\tau_{corr} = 3$ (middle curves), and $\tau_{corr} = 10$ ms (upper curves). Continuous lines are drawn in *b* and *c* only and correspond to Equations 6.17 and 6.22.

large enough; otherwise, it increased without bound. In addition, the increase in firing rate as a function of correlation time depended strongly on the relative values of μ and σ , with higher μ making the difference smaller.

Key to obtaining the analytic results was the use of a binary input. It is thus reasonable to ask whether the trends discussed above depend critically on the discrete nature of the binary variable. Gaussian white noise can be properly approximated with a binary variable because of the central limit theorem. As a consequence, the results for the model without leak were identical when the input was uncorrelated and either gaussian or binary. With correlated noise, the input current fluctuates randomly between a positive and a negative state, and the dwell time in each state is distributed exponentially. If instead of a binary variable a gaussian variable is used, with identical statistics for its sign, the results differ somewhat but are qualitatively the same for the two models: for example, the rate still increases as a function of correlation time, and the same asymptotic behaviors are seen (data not shown).

Here, we considered the response of the model neuron as a function of the total integrated input, but a real neuron actually responds to a set of incoming spike trains. Ideally, one would like to determine how the statistics

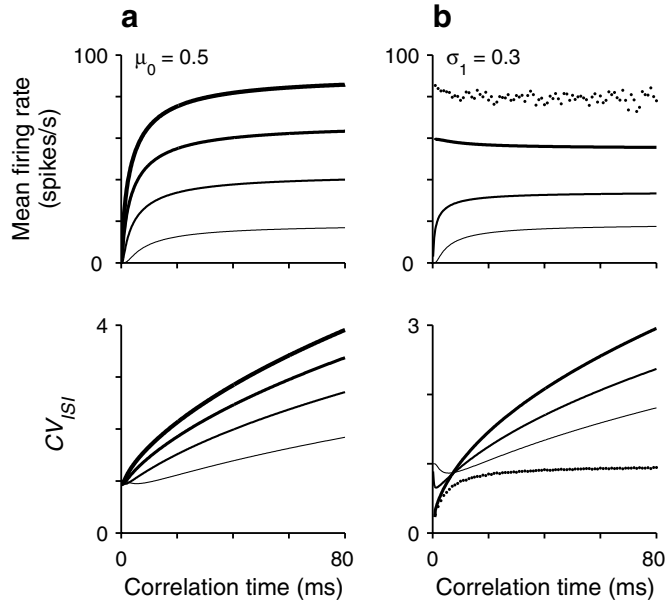


Figure 12: Responses of the leaky integrate-and-fire neuron as functions of the correlation time τ_{corr} . Analytic results are shown as continuous lines; dots are from simulations. Plots on the top and bottom rows show the mean firing rate and CV_{ISI} , respectively. (a) The four curves shown in each plot correspond to four values of σ_1 : 0.55, 0.8, 1.1, and 1.4, with thicker lines corresponding to higher values. For all these curves, $\mu_0 = 0.5$, as indicated. (b) The four traces in each plot correspond to four values of μ_0 : 0.75, 0.9, 1.15, and 1.31 (dots), with thicker lines corresponding to higher values. For these curves, $\sigma_1 = 0.3$, as indicated. As the correlation time increases, the firing rate tends to an asymptotic value. In contrast, the CV_{ISI} diverges always, except when the threshold V_θ (equal to 1) is below $\mu_0 - \sigma_1$; this case corresponds to the dots in *b*.

of the hundreds or thousands of incoming spike trains relate to the mean, variance, and correlation time of the integrated input current, but in general this is difficult. Methods based on a population density analysis have been applied to similar problems (Nykamp & Tranchina, 2000; Haskell et al., 2001). These methods are also computationally intensive, but eventually may be optimized to compute efficiently the spiking statistics of more accurate models. In a previous study (Salinas & Sejnowski, 2000), we investigated how the firing rates and correlations of multiple input spike trains affected the mean and standard deviation of the total input (and ultimately the statistics of the response), but this required certain approximations. In particular, we implicitly assumed that the correlation time of the resulting

integrated input was negligible. This is a good approximation when the correlations between input spike trains have a timescale shorter than the synaptic time constants, so that the latter determine the correlation time of the integrated input (Svirskis & Rinzel, 2000). But this may not be always true, as discussed below.

In the cortex, correlations between input spike trains are to be expected simply because of the well-known convergent and divergent patterns of connectivity (Braitenberg & Schüz, 1997): neurons that are interconnected or receive common input should be correlated. This has been verified through neurophysiological experiments in which pairs of neurons are recorded simultaneously and their cross-correlation histograms are calculated. The widths of these measured cross-correlograms may go from a few to several hundred milliseconds, for both neighboring neurons in a single cortical area (Gochin, Miller, Gross, & Gerstein, 1991; Brosch & Schreiner, 1999; Steinmetz et al., 2000) and neurons in separate areas (Nelson et al., 1992). Thus, such correlation times may be much longer than the timescales of common AMPA and GABA-A synapses (Destexhe, Mainen, & Sejnowski, 1998). Neurons typically fire action potentials separated by time intervals of the same orders of magnitude—a few to hundreds of milliseconds—so under normal circumstances, there may be a large overlap between the timescales of neuronal firing and input correlation. This is precisely the situation in which correlations should not be ignored; if in this case the inputs to a neuron are assumed to be independent, a crucial component of its dynamics may be overlooked. Although not explicitly included here, concerted oscillations between inputs may have a dramatic impact on a postsynaptic response too (Salinas & Sejnowski, 2000). This alternate form of correlated activity is also ubiquitous among cortical circuits (Singer & Gray, 1995; Fries et al., 2001).

The results support the idea that input correlations represent a major factor in determining the variability of a neuron (Gur, Beylin, & Snodderly, 1997; Stevens & Zador, 1998; Destexhe & Paré, 2000; Salinas & Sejnowski, 2000), especially in the case of a CV_{ISI} higher than 1 (Svirskis & Rinzel, 2000). However, integrative properties (Softky & Koch, 1993; Shadlen & Newsome, 1994) and other intrinsic cellular mechanisms (Wilbur & Rinzel, 1983; Troyer & Miller, 1997; Gutkin & Ermentrout, 1998) play important roles too.

In many respects, the model neurons used here are extremely simple: they do not include an extended morphology or additional intrinsic, voltage-dependent currents that may greatly expand their dynamical repertoire. However, the results may provide some intuition on the effects produced by the correlation timescale of the input. For instance, a given firing rate can be obtained with either high or low output variability depending on the relative values of μ , σ , and τ_{corr} . This distinction between regular and irregular firing modes may be useful even under more realistic conditions (Bell, Mainen, Tsodyks, & Sejnowski, 1995; Troyer & Miller, 1997; Hó & Destexhe, 2000; Salinas & Sejnowski, 2000).

A challenge lying ahead is extending the techniques used here to network interactions (Nykamp & Tranchina, 2000; Haskell et al., 2001). This requires solving coupled equations for the firing probability densities of multiple, interconnected neurons. This problem is not trivial mathematically or computationally, but it may lead to a better understanding of network dynamics based on a solid statistical foundation.

Appendix A: Generating Correlated Binary Samples _____

Here we describe how the correlated binary input with zero mean, unit variance, and exponential correlation function was implemented in the simulations. The sequence of correlated binary samples was generated through the following recipe:

$$Z_{i+1} = Z_i \text{sign}(P_s - u_{i+1}), \quad (\text{A.1})$$

where Z_i is the sample at the i th time step, $P_s = 1 - P_c = 1 - \Delta t / (2\tau_{corr})$, and u is a random number, independent of Z , uniformly distributed between 0 and 1 (Press, Flannery, Teukolsky, & Vetterling, 1992). The initial value Z_0 may be either +1 or -1. Note that the probability that $\text{sign}(P_s - u)$ is positive equals P_s ; therefore,

$$P(Z_{i+1} = +1) = P(Z_i = +1)P_s + P(Z_i = -1)P_c, \quad (\text{A.2})$$

because u is chosen independent of the Z samples. Assuming that $P(Z_{i+1} = +1) = P(Z_i = +1)$, it follows from the above relation that $P(Z_i = +1) = 1/2$, and therefore that the mean of the sequence is zero. Showing that the variance of Z equals one is trivial: simply square both sides of equation A.1 to find that Z^2 is always equal to one.

Regarding the correlation function, the main result is that

$$\overline{Z_i Z_{i+j}} = (P_s - P_c)^j, \quad j \geq 0. \quad (\text{A.3})$$

This can be seen by induction. First compute the correlation between two consecutive samples by multiplying equation A.1 by Z_i , so that

$$\overline{Z_i Z_{i+1}} = \overline{Z_i^2 \text{sign}(P_s - u_{i+1})} = P_s - P_c. \quad (\text{A.4})$$

The last step follows because $\text{sign}(P_s - u)$ is positive a fraction P_s of the time. This expression shows that equation A.3 is valid for $j = 1$; now assume that it is valid for indices i and j , and compute the correlation between samples i and $i + j + 1$:

$$\overline{Z_i Z_{i+j+1}} = \overline{Z_i Z_{i+j} \text{sign}(P_s - u_{i+j+1})} = (P_s - P_c)^{j+1}. \quad (\text{A.5})$$

Therefore, equation A.3 is true for all $j \geq 0$. Analogous results can be obtained for $j < 0$ as well. Finally, note that equation A.3 means that the correlation between Z samples is an exponential. Furthermore,

$$(P_s - P_c)^j = \left(1 - \frac{\Delta t}{\tau_{corr}}\right)^{\frac{j}{\Delta t}}, \quad (\text{A.6})$$

because $P_s = 1 - P_c$ and because the time lag t is equal to $j\Delta t$. In the limit when $\Delta t \rightarrow 0$, the above expression becomes an exponential function equal to equation 3.5.

Appendix B: Generating Correlated Gaussian Samples _____

Here we describe how a correlated gaussian input with zero mean, unit variance, and exponential correlation function can be implemented in computer simulations. The sequence of correlated gaussian samples was generated through the following recipe:

$$W_{i+1} = \epsilon W_i + \sqrt{1 - \epsilon^2} g_{i+1}, \quad (\text{B.1})$$

where

$$\epsilon \equiv \exp\left(-\frac{\Delta t}{\tau_{corr}}\right), \quad (\text{B.2})$$

and g is a random number independent of W , drawn from a gaussian distribution with zero mean and unit variance (Press et al., 1992). The g samples are uncorrelated. Applying equation B.2 iteratively and setting the initial value W_0 equal to ϵg_0 , we find

$$W_N = \epsilon^N g_0 + \sqrt{1 - \epsilon^2} \sum_{i=0}^{N-1} \epsilon^i g_{N-i}. \quad (\text{B.3})$$

Averaging over the distribution of g on both sides implies that the mean of W equals zero, because all g samples have an expected value of zero. By squaring the above equation and then averaging, we obtain

$$\overline{W_N^2} = \epsilon^{2N} \overline{g_0^2} + (1 - \epsilon^2) \sum_{i,j=0}^{N-1} \epsilon^{i+j} \overline{g_{N-i} g_{N-j}} = 1. \quad (\text{B.4})$$

In the last step, we used the fact that the g samples are uncorrelated, so that $\overline{g_{N-i} g_{N-j}} = \delta_{ij}$, where δ_{ij} is equal to 1 whenever $i = j$ and is 0 otherwise. Also, we used the standard result for the sum of N terms of a geometric series (Jeffrey, 1995).

The correlation function can be determined by induction, as in the case of binary samples. To prove that

$$\overline{W_i W_{i+j}} = \epsilon^j, \quad j \geq 0, \quad (\text{B.5})$$

first compute the correlation between two consecutive samples by multiplying equation B.1 by W_i , so that

$$\overline{W_i W_{i+1}} = \epsilon \overline{W_i^2} + \sqrt{1 - \epsilon^2} \overline{W_i g_{i+1}} = \epsilon. \quad (\text{B.6})$$

The last step follows again because g is independent of the W samples. This shows that equation B.5 is valid for $j = 1$. Now assume that it is valid for samples i and $i + j$, and compute the correlation for samples i and $i + j + 1$:

$$\overline{W_i W_{i+j+1}} = \epsilon \overline{W_i W_{i+j}} + \sqrt{1 - \epsilon^2} \overline{W_i g_{i+j+1}} = \epsilon^{j+1}. \quad (\text{B.7})$$

Therefore, equation B.5 is true for all $j \geq 0$. The analogous results for $j < 0$ can be obtained similarly. Recalling the definition of ϵ and that $t = j\Delta t$, the right-hand side of equation B.5 becomes

$$\exp\left(-\frac{|t|}{\tau_{corr}}\right). \quad (\text{B.8})$$

Finally, note that uncorrelated samples may be produced by setting $\epsilon = 0$ in equation B.1, which is useful for switching between correlated and uncorrelated noise models in the simulations.

Appendix C: Simulation Methods

Performing computer simulations of the models described in the main text is straightforward. The key is that the discretized equations, 4.1, 5.1, and 6.6 can be included literally in the simulation software. To run a simulation, first, values for μ_0 , σ_0 (or σ_1), τ , and τ_{corr} are chosen, as well as a time step Δt . At the start of each spike cycle, T is set to zero and V is set equal to V_{reset} . Thereafter, on each time step, T is increased by Δt , a new value of Z is generated according to equation A.1, and V is updated according to the discretized equation for the model being simulated, for instance, equation 5.1 for the nonleaky integrate-and-fire neuron driven by correlated binary noise. For models without leak, the barrier needs to be checked on every step. If after the update V becomes negative, then it is set to zero. The updating continues until threshold is exceeded, in which case a spike is recorded, the value of T is saved, and a new spike cycle is started. Simulations in which the model neuron was driven by a gaussian input proceeded exactly in the same way as with a binary input, except that equation B.1 was used to generate correlated gaussian numbers W , and Z in the discretized equations was replaced by W .

In all simulations presented here, we used $\tau = 10$ ms, $V_\theta = 1$, and $V_{reset} = 1/3$ (in arbitrary units). The integration time step Δt varied between 0.1 and 0.001 ms. Average values of T and T^2 for each condition tested were computed after 1,000 spike cycles for uncorrelated noise and 2,000 cycles for correlated noise. All interspike interval histograms shown include about 4,500 spikes. Matlab scripts that implement the models presented here, along with functions that evaluate the analytic solutions, may be found on-line at <http://www.cnl.salk.edu/~emilio/code.html>.

Acknowledgments

This research was supported by the Howard Hughes Medical Institute. We thank Bill Bialek for comments on earlier results, motivating this work. We also thank Dan Tranchina for many corrections and invaluable guidance in the analysis and Larry Abbott and Paul Tiesinga for helpful comments.

References

- Bell, A. J., Mainen, Z. F., Tsodyks, M., & Sejnowski, T. J. (1995). "Balancing" of conductances may explain irregular cortical spiking (Tech. Rep. No. INC-9502). San Diego, CA: Institute for Neural Computation, University of California.
- Berg, H. C. (1993). *Random walks in biology*. Princeton, NJ: Princeton University Press.
- Braitenberg, V., & Schüz, A. (1997). *Cortex: Statistics and geometry of neuronal connectivity*. Berlin: Springer.
- Brosch, M., & Schreiner, C. E. (1999). Correlations between neural discharges are related to receptive field properties in cat primary auditory cortex. *Eur. J. Neurosci.*, *11*, 3517–3530.
- Burkitt, A. N., & Clark, G. M. (1999). Analysis of integrate-and-fire neurons: Synchronization of synaptic input and spike output. *Neural Comput.*, *11*, 871–901.
- Dayan, P., & Abbott, L. F. (2001). *Theoretical neuroscience*. Cambridge, MA: MIT Press.
- Destexhe, A., Mainen, Z. F., & Sejnowski, T. J. (1998). Kinetic models of synaptic transmission. In C. Koch & I. Segev (Eds.), *Methods in neuronal modeling* (2nd ed., pp. 1–25). Cambridge, MA: MIT Press.
- Destexhe, A., & Paré, D. (2000). A combined computational and intracellular study of correlated synaptic bombardment in neocortical pyramidal neurons in vivo. *Neurocomputing*, *32–33*, 113–119.
- Diesmann, M., Gewaltig, M.-O., & Aertsen, A. (1999). Stable propagation of synchronous spiking in cortical neural networks. *Nature*, *402*, 529–533.
- Feng, J., & Brown, D. (2000). Impact of correlated inputs on the output of the integrate-and-fire model. *Neural Comput.*, *12*, 671–692.
- Feynman, R. P., Leighton, R. B., & Sands, M. (1963). *The Feynman lectures on physics* (Vol. 1). Reading, MA: Addison-Wesley.

- Fries, P., Reynolds, J. H., Rorie, A. E., & Desimone, R. (2001). Modulation of oscillatory neuronal synchronization by selective visual attention. *Science*, *291*, 1560–1563.
- Gardiner, C. W. (1985). *Handbook of stochastic methods for physics, chemistry and the natural sciences*. Berlin: Springer.
- Gerstein, G. L., & Mandelbrot, B. (1964). Random walk models for the spike activity of a single neuron. *Biophys J.*, *4*, 41–68.
- Gochin, P. M., Miller, E. K., Gross, C. G., Gerstein, G. L. (1991). Functional interactions among neurons in inferior temporal cortex of the awake macaque. *Exp. Brain. Res.*, *84*, 505–516.
- Gur, M., Beylin, A., & Snodderly, D. M. (1997). Response variability of neurons in primary visual cortex (V1) of alert monkeys. *J. Neurosci.*, *17*, 2914–2920.
- Gutkin, B. S., & Ermentrout, G. B. (1998). Dynamics of membrane excitability determine interspike interval variability: A link between spike generation mechanisms and cortical spike train statistics. *Neural Comput.*, *10*, 1047–1065.
- Haskell, E., Nykamp, D. Q., & Tranchina, D. (2001). Population density methods for large-scale modelling of neuronal networks with realistic synaptic kinetics: Cutting the dimension down to size. *Network*, *12*, 141–174.
- Hô, N., & Destexhe, A. (2000). Synaptic background activity enhances the responsiveness of neocortical pyramidal neurons. *J. Neurophysiol.*, *84*, 1488–1496.
- Jeffrey, A. (1995). *Handbook of mathematical formulas and integrals*. London: Academic Press.
- Kisley, M. A., & Gerstein, G. L. (1999). The continuum of operating modes for a passive model neuron. *Neural Comput.*, *11*, 1139–1154.
- Maršálek, P., Koch, C., Maunsell, J. (1997). On the relationship between synaptic input and spike output jitter in individual neurons. *Proc. Natl. Acad. Sci. USA*, *94*, 735–740.
- Nelson, J. I., Salin, P. A., Munk, M.H.-J., Arzi, M., & Bullier, J. (1992). Spatial and temporal coherence in cortico-cortical connections: A cross-correlation study in areas 17 and 18 in the cat. *Vis. Neurosci.*, *9*, 21–37.
- Nykamp, D. Q., & Tranchina, D. (2000). A population density approach that facilitates large-scale modeling of neural networks: Analysis and an application to orientation tuning. *J. Comput. Neurosci.*, *8*, 19–50.
- Press, W. H., Flannery, B. P., Teukolsky, S. A., & Vetterling, W. T. (1992). *Numerical recipes in C*. Cambridge: Cambridge University Press.
- Ricciardi, L. M. (1977). *Diffusion processes and related topics in biology*. Berlin: Springer-Verlag.
- Ricciardi, L. M. (1995). Diffusion models of neuron activity. In M. Arbib (Ed.), *Handbook of brain theory and neural networks* (pp. 299–304). Cambridge, MA: MIT Press.
- Ricciardi, L. M., & Sacerdote, L. (1979). The Ornstein-Uhlenbeck process as a model for neuronal activity. *Biol. Cybern.*, *35*, 1–9.
- Ricciardi, L. M., & Sato, S. (1988). First-passage-time density and moments of the Ornstein-Uhlenbeck process. *J. Appl. Prob.*, *25*, 43–57.
- Risken, H. (1996). *The Fokker-Planck equation: Methods of solution and applications* (2nd ed.). Berlin: Springer-Verlag.

- Salinas, E., & Sejnowski, T. J. (2000). Impact of correlated synaptic input on output firing rate and variability in simple neuronal models. *J. Neurosci.*, *20*, 6193–6209.
- Salinas, E., & Sejnowski, T. J. (2001). Correlated neuronal activity and the flow of neural information. *Nat. Rev. Neurosci.*, *2*, 539–550.
- Shadlen, M. N., & Newsome, W. T. (1994). Noise, neural codes and cortical organization. *Curr. Opin. Neurobiol.*, *4*, 569–579.
- Shinomoto, S., Sakai, Y., & Funahashi, S. (1999). The Ornstein-Uhlenbeck process does not reproduce spiking statistics of neurons in prefrontal cortex. *Neural Comput.*, *11*, 935–951.
- Singer, W., & Gray, C. M. (1995). Visual feature integration and the temporal correlation hypothesis. *Annu. Rev. Neurosci.*, *18*, 555–586.
- Smith, C. E. (1992). A heuristic approach to stochastic models of single neurons. In T. McKenna, J. L. Davis, & S. F. Zornetzer (Eds.), *Single neuron computation* (pp. 561–588). Cambridge, MA: Academic Press.
- Softky, W. R., & Koch, C. (1993). The highly irregular firing of cortical cells is inconsistent with temporal integration of random EPSPs. *J. Neurosci.*, *13*, 334–350.
- Steinmetz, P. N., Roy, A., Fitzgerald, P. J., Hsiao, S. S., Johnson, K. O., & Niebur, E. (2000). Attention modulates synchronized neuronal firing in primate somatosensory cortex. *Nature*, *404*, 187–190.
- Stevens, C. F., & Zador, A. M. (1998). Input synchrony and the irregular firing of cortical neurons. *Nature Neurosci.*, *1*, 210–217.
- Svirskis, G., & Rinzel, J. (2000). Influence of temporal correlation of synaptic input on the rate and variability of firing in neurons. *Biophys. J.*, *79*, 629–637.
- Thomas, M. U. (1975). Some mean first-passage time approximations for the Ornstein-Uhlenbeck process. *J. Appl. Prob.*, *12*, 600–604.
- Tiesinga, P. H. E., José, J. V., & Sejnowski, T. J. (2000). Comparison of current-driven and conductance-driven neocortical model neuron with Hodgkin-Huxley voltage-gated channels. *Phys. Rev. E.*, *62*, 8413–8419.
- Troyer, T. W., & Miller, K. D. (1997). Physiological gain leads to high ISI variability in a simple model of a cortical regular spiking cell. *Neural Comput.*, *9*, 971–983.
- Tuckwell, H. C. (1988). *Introduction to theoretical neurobiology*. Cambridge: Cambridge University Press.
- Tuckwell, H. C. (1989). *Stochastic processes in the neurosciences*. Philadelphia: Society for Industrial and Applied Mathematics.
- Uhlenbeck, G. E., & Ornstein, L. S. (1930). On the theory of Brownian motion. *Phys. Rev.*, *36*, 823–841.
- Van Kampen, N. G. (1981). *Stochastic processes in physics and chemistry*. Amsterdam: North-Holland.
- Wilbur, W. J., & Rinzel, J. (1983). A theoretical basis for large coefficient of variation and bimodality in neuronal interspike interval distribution. *J. Theo. Biol.*, *105*, 345–368.